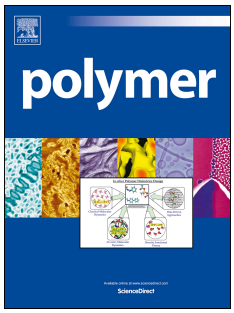

Synthesis and fabrication of lightweight microcellular thermoplastic polyimide foams using supercritical CO_2 foaming

Haiming Liu, Xiangdong Wang, Hao-Yang Mi, Maxwell Fordjour Antwi-Afari, Chuntai Liu

PII: S0032-3861(23)00878-9

DOI: https://doi.org/10.1016/j.polymer.2023.126548

Reference: JPOL 126548

To appear in: *Polymer*

Received Date: 8 July 2023

Revised Date: 24 October 2023

Accepted Date: 26 November 2023

Please cite this article as: Liu H, Wang X, Mi H-Y, Antwi-Afari MF, Liu C, Synthesis and fabrication of lightweight microcellular thermoplastic polyimide foams using supercritical CO_2 foaming, *Polymer* (2024), doi: https://doi.org/10.1016/j.polymer.2023.126548.

Synthesis and fabrication of lightweight microcellular thermoplastic polyimide foams using supercritical CO_2 foaming

Haiming Liu [a], Xiangdong Wang [c], Hao-Yang Mi [a,b*], Maxwell Fordjour Antwi-Afari [d], Chuntai Liu [a,b**]

[a] *School of Materials Science and Engineering, Zhengzhou University, Zhengzhou, Henan, 450001 People's Republic of China*

[b] *Key Laboratory of Materials Processing & Mold, Ministry of Education; National Engineering Research Center for Advanced Polymer Processing Technology, Zhengzhou University, Zhengzhou, Henan, 450001, People's Republic of China*

[c] *School of Chemistry and Materials Engineering, Beijing Technology and Business University, Beijing, 100048, People's Republic of China*

[d] *Department of Civil Engineering, College of Engineering and Physical Sciences, Aston University, Birmingham, B4 7ET, United Kingdom*

CRediT authorship contribution statement

Haiming Liu: Conceptualization, Data curation, Formal analysis, Methodology, Investigation, Methodology, Writing – original draft, Writing – review & editing. **Xiangdong Wang**: Conceptualization, Supervision, Validation. **Hao-Yang Mi**: Formal analysis, Investigation, Validation, Funding acquisition, Writing – review. **Maxwell Fordjour Antwi-Afari**: Writing – review & editing, formal analysis. **Chuntai Liu**: Supervision, Validation, Funding acquisition.

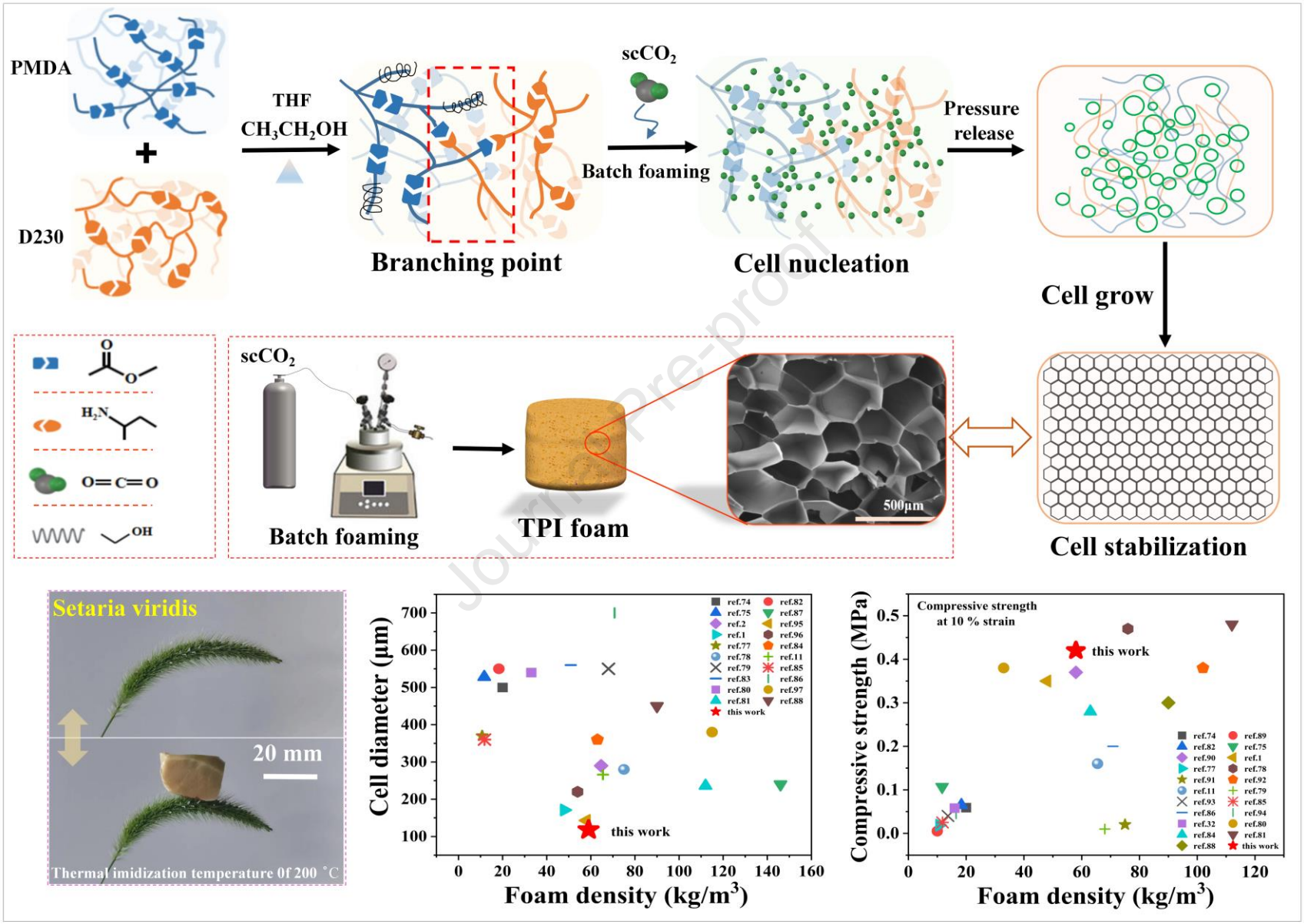
PMDA
D230
THF
CH_3CH_2OH
Branching point
$scCO_2$
Batch foaming
Cell nucleation
Pressure release
Cell grow
Cell stabilization
$scCO_2$
Batch foaming
TPI foam
500μm
Setaria viridis
20 mm
Thermal imidization temperature 0f 200 °C
Cell diameter (μm)
Foam density (kg/m³)
this work
Compressive strength at 10 % strain
Compressive strength (MPa)
Foam density (kg/m³)
this work

Synthesis and fabrication of lightweight microcellular thermoplastic polyimide foams using supercritical CO_2 foaming

Haiming Liu [a], Xiangdong Wang [c], Hao-Yang Mi [a,b*], Maxwell Fordjour Antwi-Afari [d], Chuntai Liu [a,b**]

[a] *School of Materials Science and Engineering, Zhengzhou University, Zhengzhou, Henan, 450001 People's Republic of China*

[b] *Key Laboratory of Materials Processing & Mold, Ministry of Education; National Engineering Research Center for Advanced Polymer Processing Technology, Zhengzhou University, Zhengzhou, Henan, 450001, People's Republic of China*

[c] *School of Chemistry and Materials Engineering, Beijing Technology and Business University, Beijing, 100048, People's Republic of China*

[d] *Department of Civil Engineering, College of Engineering and Physical Sciences, Aston University, Birmingham, B4 7ET, United Kingdom*

*** Corresponding author.**

School of Materials Science and Engineering, Zhengzhou University, Zhengzhou, Henan, 450001 People's Republic of China

Key Laboratory of Materials Processing & Mold, Ministry of Education; National Engineering Research Center for Advanced Polymer Processing Technology, Zhengzhou University, Zhengzhou, Henan, 450001, People's Republic of China

E-mail address: mihaoyang@zzu.edu.cn (H. Mi) and ctliu@zzu.edu.cn (C. Liu)

ABSTRACT

Polyimide foams (PIFs) are usually synthesized by solution polymerization, followed by chemical foaming to prepare thermosetting foam. In this research, lightweight microcellular thermoplastic polyimide foams (TPIFs) were fabricated via a novel two-step foaming approach using supercritical carbon dioxide ($scCO_2$) as a blowing agent. The poly(amic acid) (PAA) and polyester ammonium salt (PEAS) precursor solutions were synthesized with pyromellitic dianhydride (PMDA) as dianhydride reagents and polyether amine Jeffamine D230 as aliphatic diamine reagent via blending and solution polymerization, respectively. The solution polymerization process demonstrated a higher molecular weight and superior formability than the blending process. The optimum thermal imidization temperature of 200 °C was optimized via the thermal and rheological property analysis. The cell morphology and mechanical properties of the TPIFs could be turned by varying the saturation time, foaming pressure, and imidization temperature. At a thermal imidization temperature of 200 °C, the TPIFs exhibited a branched structure with a small mean cell diameter (123.78 μm), and a high compressive strength (0.4 MPa) under 10 % strain at high temperature and pressure, which was more than ten times that of the TPIFs with thermal imidization temperature of 130 °C. This research provides a feasible method for producing high volume expansion ratio TPIFs with adjustable microcellular structures and outstanding mechanical properties.

Keywords: Thermoplastic polyimide foams; Thermal imidization; Supercritical carbon dioxide; Compressive strength

1. Introduction

In recent years, polymeric foams have been widely concerned in aerospace, electronic engineering, transportation, and fuel cells owing to their remarkable performances, such as lightweight, cushioning, shock absorption, sound absorption, and thermal insulation [1-3]. Prevalent polymer foams including polypropylene, polyethylene, polystyrene, polyurethane, polyvinyl chloride, etc, are generally vulnerable to heat and fire, which cannot meet the strict requirements of high-end engineering applications [4-6]. Therefore, a great effort has been devoted to develop special foams such as polyimide (PI) foams, polymethacrylimide foams, and expanded polycarbonate foams which can suit the stringent needs of special engineering applications.

As a new type of ultra-high-performance engineering plastic, the skeleton of the polyimide chain contains an imide and benzene ring, which gives the material sensational thermal stability and mechanical properties, flame retardancy, and chemical resistance, etc. Polyimide foams (PIFs), a kind of polymer foams with a wide variety, are mainly composed of PI resin and internal open or closed porous structures of different sizes [7-9]. Du Pont and Monsanto first produced and commercialized them using PI precursor polyamic acids in the late 1960s [10-12]. Subsequently, the launch of commercial PIFs such as Solimide®, TEEK®, and Rexfoam® has dramatically expanded the global market as thermal insulation materials in high-end applications [13,14]. PIFs have been developed to the rapid demand to improve energy efficiency in advanced domains, thanks to their unexceptionable balance of mechanical, dielectric, and thermal properties, which have made them irreplaceable in various applications, including aerospace, battleship, microelectronic, and wearable devices [15,16].

A typical preparation of PIFs is as follows: 1) polyamide acid (PAA) solution or polyester ammonium salt (PEAS) is synthesized by low-temperature polycondensation of dianhydride and diamine in polar solvents such as dimethyl formamide (DMF), dimethylacetamide (DMAc), N-Methylpyrrolidone (NMP) or tetrahydrofuran (THF)/methanol(MeOH) mixed solvents; 2) PAAs or PEAS is dried into precursor powders under vacuum/or foamed directly by using the freeze-dried method; 3) PIFs are obtained by heating precursor particles which utilize residual solvent and minor molecule by-products as blowing agent during the process [17,18]. The two monomers of dianhydride and diamine have vast sources of raw materials, low toxicity, and accessible synthesis compared to other heterocyclic polymer monomers, such as polybenzimidazole, polybenzoxazole, polybenzothiazole, and polyquinoline. The diversity in monomer types allows for unlimited possibilities to develop PIFs for a wide range of properties [19,20]. Nevertheless, PIFs are usually synthesized by thermosetting and chemical foaming, but this approach is environmentally toxic, and it is difficult to regulate the cell structure, remold the foam, and no fundamental research focused on preparing thermoplastic polyimide foams

(TPIFs). In addition, the synthesis process for thermosetting PIFs usually takes a long time, which comprises the formation of the PAA or PEAS (6 h [18]), solvent removal, and the imidization reaction (2h [21]). Producing PIFs through an efficient approach is still challenging.

According to the state of PI precursor polymer, various methods have been developed and proposed to fabricate PIFs, such as solution freeze-dried foaming [22,23], precursor powder foaming [24,25], three-dimensional (3D) printing [26,27], microsphere foaming [28-30], isocyanate-based PI foaming method [31,32]. Among them, the precursor powder foaming and freeze-dried method have been widely employed to prepare high temperature-resistant thermosetting polyimide-based foams [33,34]. Ni et al. [1] obtained BTDA-derived polyimide rigid foam with different diamine structures via the PAA powders foaming method. The results revealed that the prepared semi-rigid PIFs demonstrate outstanding potential for thermal insulation and structural support applications. However, it is difficult to control the homogeneity of the foam. Liu et al. [35] prepared a series of lamellar-structured graphene based PI aerogels with unprecedented thermal conduction capacity using the freeze-drying forming method. According to this work, the foam has a relatively low density and excellent thermal conductivity. However, poor mechanical performance limited its application. Luo et al. [30] fabricated polyimide microsphere foam with the bulk density varying from 56.9 to 132.2 kg/m^3 by microsphere foaming. Liu et al. [36] presented polyimide closed-cell stochastic foams with tunable densities using the method of three-dimensional (3D) direct ink printing filaments. Compared to other methods, the 3D printing process had an unparalleled advantage in preparing sophisticated equipment with arbitrary shapes and excellent interface bonding performances. Ma et al. [37] prepared open-cellular PIFs with a low density of 0.014~0.022 g/cm^3 using an isocyanate-based PI foaming method. However, those methods were relatively complex and inefficient owing to their reliance on conventional molding technologies, which increased their costs. Therefore, it was a great challenge to realize large-scale industrialization because of the time-consuming nature, low efficiency, and high cost of raw materials for the chemical foaming process. Therefore, an efficient and cost-effective method for producing PIFs is urgently required.

Supercritical fluid (SCF) foaming is a novel foaming technique that uses physical blowing agents to produce porous polymer materials under high temperature and pressure conditions [38,39]. Because SCF foaming does not require chemical agents, it is environmentally friendly. This makes it an ideal method for the preparation of micro and nanoporous foams [40-42]. Supercritical carbon dioxide ($scCO_2$) as an abundant inert gas is commonly used in SCF foaming due to its low cost, wide availability, high diffusion rate, cell adjustability, and nontoxicity [43-45]. However, since the foaming of rigid microcellular TPIFs requires delicate melt strength control to prevent cell collapse and realize a high expansion ratio, relevant research on the $scCO_2$ foaming TPIFs is limited.

In this research, we proposed a novel and effective two-step foaming approach to fabricate high-strength TPIFs. PAAs were prepared using pyromellitic dianhydride (PMDA) as dianhydride reagents, Jeffamine D230 as aliphatic diamine reagent via blending without any solvent and thermal imidization treatment. Meanwhile, the PEAS was also synthesized using PMDA and Jeffamine D230 with a corresponding additive by solution polymerization. Subsequently, the blending and conventional solution polymerization processes were compared to the characteristics of the polymer, followed by $scCO_2$ batch foaming. The chemical structure and the imidization reaction kinetics of the polyimides were investigated by Fourier transform infrared (FTIR) and ^{13}C nuclear magnetic resonance (NMR) spectroscopies. The average molar masses, glass transition temperatures, thermal behavior, and rheological properties were additionally reported to fully describe the obtained polyimides. The cell structure and mechanical performance of TPIFs can be regulated by adjusting the thermal imidization temperature. From the perspective of this article, an innovative TPIF material and a sustainable scalable $scCO_2$ foaming method are developed.

2. Experimental

2.1. Materials

Pyromellitic dianhydride (PMDA, ≥ 97 %) powder, as an effective dianhydride, was obtained from Sigma-Aldrich Chemical Co. Ltd, USA. Before synthesis, PMDA powder was dried in a vacuum oven at 80 °C for 12 h to remove the influence of moisture on the experiment. Jeffamine D230, as a new amine compound, was kindly provided by Huntsman. 2-Methylimidazole (98 %) was used as a catalyst from Aladdin. Tetrahydrofuran (THF) and anhydrous ethanol (EtOH, ≥ 99.7 %), used as a solvent, were supplied by MREDA Technology Co. Ltd, USA, and Energy Chemical Co. Ltd, China, respectively. Supercritical carbon dioxide ($scCO_2$) with a purity of 99.999 % was acquired from Air Liquide Co. Ltd, China. All commercial reagents in this research were analytical grade and used without further purification.

2.2. Preparation of poly(amic acid) (PAA) precursor solutions

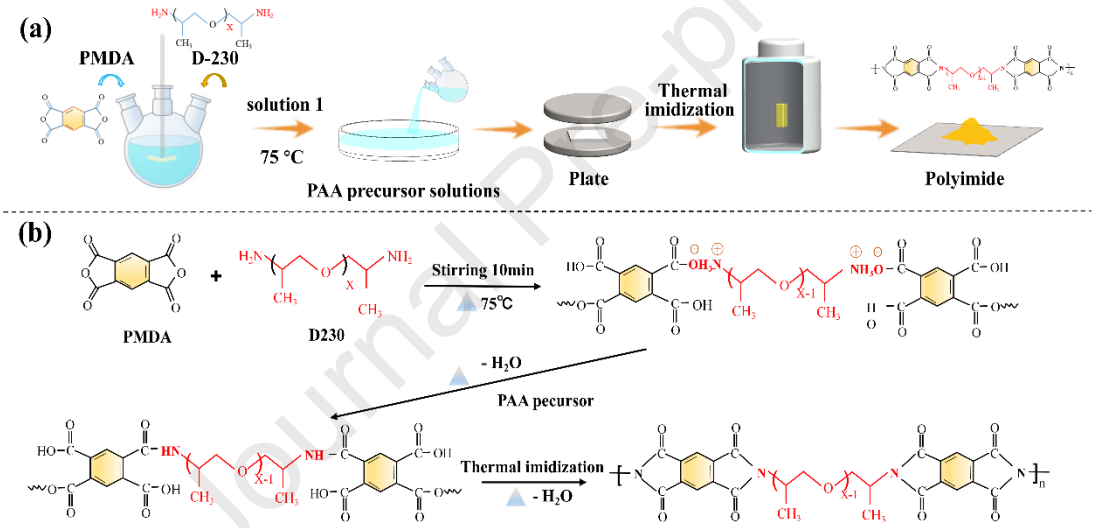

Fig. 1. (a) Schematic diagram of preparation process of polyimide (non-solvent), and (b) reaction mechanism of polyimide.

The preparation process and reaction mechanism of polyimide are shown in **Figs. 1(a-b),** respectively. The PAA precursor was prepared based on an equimolar ratio of PMDA and D230 without any solvent. The dianhydride powders (0.05 mol, 11 g) and liquid diamine (0.05 mol, 11.6 g) were blended at 75 °C for 10 min with magnetic stirring in a 100 ml round-bottom flask. Then, the reaction system was cooled to room temperature (25 °C). The PAA was introduced in a non-sealed autoclave batch. Samples of the reaction medium were collected after reacting at different temperatures for one hour (e.g. 100 °C, 130 °C, 140 °C, 160 °C, 180 °C, 200 °C, 230 °C and 280 °C).

2.3. Synthesis of polyester ammonium salt (PEAS) precursor solutions

The PEAS precursor solutions were fabricated based on an equimolar ratio of PMDA and

D230, forming PEAS precursor solutions containing ether bonds. Defined amount of PMDA (0.1 mol, 22 g) and catalyst (0.1 g) were dissolved in a mixture solvent of THF (40 g) and EtOH (80 g) at 75 °C for one hour with the aid of magnetic stirring in a 250 ml round-bottom flask under the protection of nitrogen atmosphere. Then, D230 (0.1 mol, 23 g) was added to the diacid diester solution and stirred for one hour to obtain homogeneous PEAS precursor solutions. Subsequently, extra THF and EtOH solvents were removed by rotation evaporation and the viscous PEAS precursor solutions were obtained for the preparation of thermoplastic polyimide (TPI) and TPIFs.

2.4. Fabrication of thermoplastic polyimide foams

A series of TPIFs with different thermally imidized reaction degrees (RD) were synthesized through a novel two-step fabrication strategy. In the first step, the PEAS was put into a non-sealed autoclave oven, and then TPI samples were prepared at different thermally imidization temperatures (i.e., 100 °C, 130 °C, 140 °C, 160 °C, 180 °C, 200 °C, 230 °C and 280 °C) for 1 h. Then, high-purity CO_2 was used to purify the vessel to remove the residual THF and EtOH and the water produced during the reaction. Afterward, TPI samples were placed inside the hermetic high-pressure vessel. Subsequently, scCO_2 as a blowing agent was pumped into the high-pressure vessel to prepare TPIFs under specific saturation temperature (110 °C), pressure (i.e., 8 MPa, 10 MPa, 11 MPa, 12 MPa, 15 MPa, and 20 MPa), and time (i.e., 5 min, 10 min, 30 min, and 60 min). After CO_2 was fully diffused and dissolved in the samples, the melt/gas mixture underwent a rapid pressure drop by releasing CO_2 within 1 s by opening a ball valve, and the specimens were taken out. The rapid release of CO_2 provided a driving force for cell nucleation and growth. During the whole saturation process, the pressure was maintained constantly by a syringe pump (260D, Teledyne, USA). The preparation route of TPIFs and autoclave batch foaming are illustrated in **Fig. 2(**a). **Fig. 2** (b) illustrates the reaction mechanism of TPI.

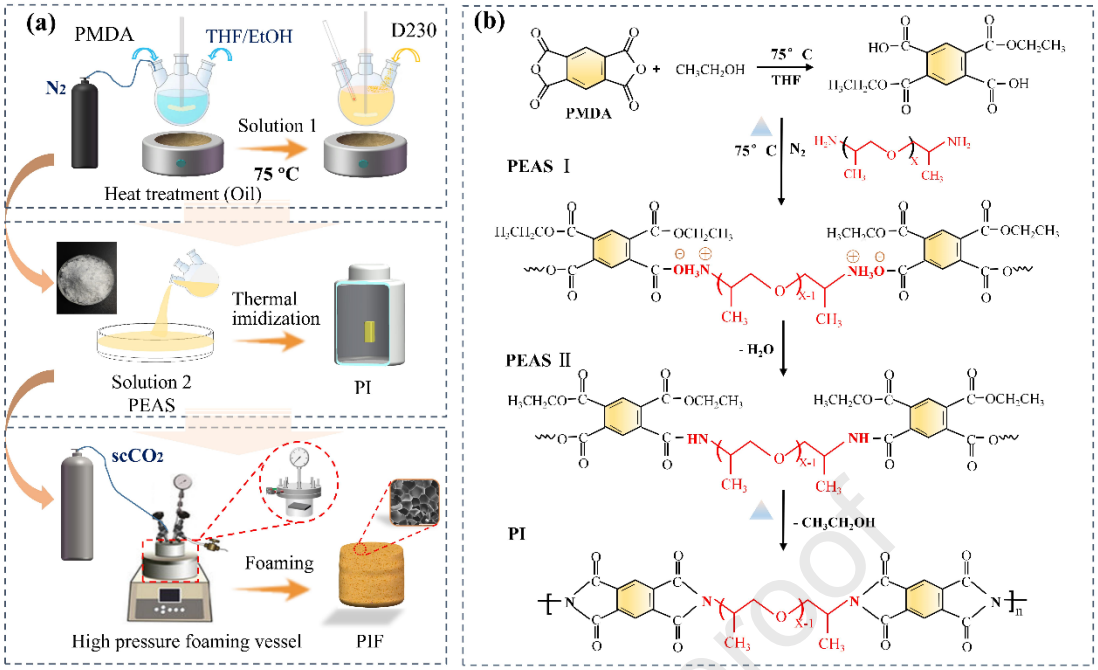

Fig. 2. (a) Schematic illustration of the two-step preparation process of PIFs and (b) the mechanism schematic diagram of PI foams.

2.5. Characterization

2.5.1. Fourier transform infrared (FTIR) spectroscopy

FTIR spectra of the polyimide samples were acquired using a Nicolet IN10MX-type FTIR spectrometer equipped with a single-refection ATR accessory over a frequency range 400-4000 cm^{-1} by collecting 32 scans. The samples were ground into powder and evenly mixed with KBr, and then the mixture was pressed into pellets for the measurement.

2.5.2. Gel permeation chromatography (GPC)

The number-average (M_n) and weight-average molecular weight (M_w) of synthetic polyimide with different thermal imidization temperature samples using THF and EtOH as solvents were tested via GPC (Agilent Technologies, 1260 Infinity IIGPC systems) with micro-storage columns at 25 °C. The appropriate mobile phase (tetrahydrofuran) was selected to dissolve PI polymers, flow through the columns at a 1 ml/min flow rate, and calibrate with polystyrene. Before testing, the dissolved samples were filtered with a membrane filter.

2.5.3. ^{13}C Nuclear magnetic resonance (^{13}C NMR)

^{13}C NMR spectra of PEAS and polyimide were recorded on a Bruker AC 250 spectrometer. The chemical shifts (δ) were expressed in a unit of ppm. The solvent was dimethyl sulfoxide d6 (DMSO-d6). NMR spectra (in DMSO-d6) were recorded on a JEOL JNM-EX400 FT/NMR spectrometer operating at 400 MHz with tetramethylsilane as a reference.

2.5.4. The thermal behavior

A differential scanning calorimeter (TA Instruments, DSC-Q100) was used to investigate the thermal behavior of the composites. The isothermal and non-isothermal desorption, glass transition temperature (Tg), and thermodynamic behavior below the decomposition temperature of the specimen were carried out under a nitrogen atmosphere. Each sample was first heated from room temperature to 300 °C at a rate of 10 °C/min to acquire the exothermic peak, isothermal for 3 minutes, then cooled the sample to 40 °C, isothermal for 3 min. Afterward, a second identical heating cycle was carried out to determine the Tg value at a 5 °C/min rate from 40 °C to 200 °C. Thermogravimetric analysis (TGA, TA thermogravimetric analyzer Q200) was carried out by heating the specimen at a rate of 10 °C/min from room temperature to 700 °C under a nitrogen atmosphere.

2.5.5. Rheological properties

A rotational rheometer (HAAKE MARS III, Germany) was used to determine the dynamic rheological properties of all samples at a test temperature of 130 °C and a frequency range of 0.1-100 rad/s. All samples were measured at 1 % of the strain range to ensure a linear viscoelastic zone. The storage modulus (G'), loss modulus (G''), loss factor (tanδ) and complex viscosity (|η*|) were measured.

2.5.6. Scanning electron microscopy (SEM)

The cellular morphologies of the cross-section of foams were characterized via a scanning electron microscope (SEM, TESCAN YEGA II, TESCAN s.r.o) at an acceleration voltage of 10 kV. Image Pro Plus software was used to count the cell size and analyze the cell density. The cell density (N_c) was calculated as follows:

$$N_c = \left(\frac{n_b}{L^2}\right)^{\frac{3}{2}} * \emptyset \quad (1)$$

$$\emptyset = \frac{\rho}{\rho_f} \quad (2)$$

Where, n_b is the number of synthetic PIF cells in the picture; L^2 (cm^2) is the area of the SEM micrograph; $\emptyset$ is the foam's volume expansion rate; ρ (g/cm^3) is the density of the un-foamed sample. ρ_f (g/cm^3) is the density of foam.

2.5.7. Mechanical properties

Compressive properties were measured using a UTM 4204 electronic universal testing machine (SUNS, China) with a 2 mm/min compressive rate according to ISO 844:2004. TPIF samples were cut to dimensions of 10 mm × 10 mm × 10 mm for the measurement, and five replicates were tested for each group.

3. Results and discussion

3.1. Synthesis of polyimides and their chemical structures

Traditional blending approach (without solvent) and solvent assisted approach were used to synthesize polyimides. The PAA precursor was obtained in the blending of dianhydride and diamine process due to the nucleophilic attack of the amino group on the carbonyl carbon of the anhydride group. The specimens acquired after the thermal imidization reaction step in the non-sealed autoclave were all amber glass-like materials, and the color gradually darkened with the increase in temperature. Their physical properties and behavior depended on the reaction temperature and time. As shown in **Figs. 3**(a-b), the synthesized PEAS powder was white, and the color changed gradually from light yellow to brown and black as the thermal imidization temperature was increased from 100 °C to 280 °C . The TPI samples had the lowest degree of branching when the thermal imidization temperature was below 130 °C at which only amide acid structure was formed. The TPI samples had a high degree of branching, and imide structures were present at 130 °C - 200 °C. The TPI samples entirely comprised imide structures, and the molecular chains broke when the temperature was higher than 230 °C. **Fig. 3** (c) shows the mechanism diagram of synthetic TPI with the presence of THF and EtOH mixing solvents, which facilitates the formation of a branched network, and should be favorable for promoting the formation of high-expansion TPIFs with stable and uniform cell structures.

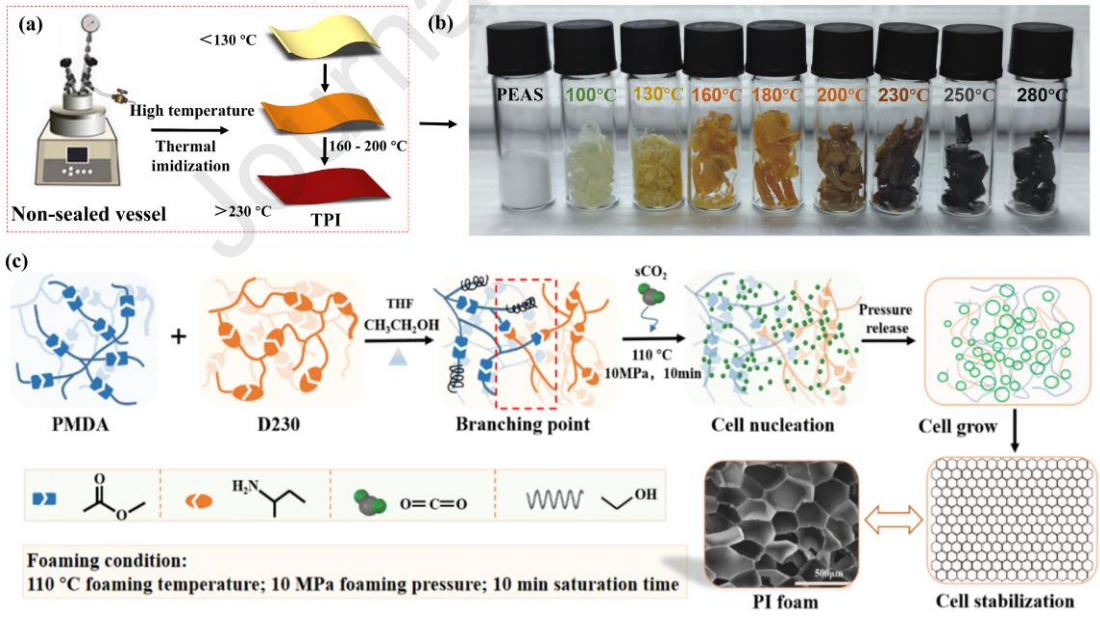

Fig. 3. Synthesize and foaming mechanism of synthetic TPIFs (a) (b) (c).

The molecular structures of the precursor polymer was investigated using FTIR spectra. The PAA precursor (**Fig. 4**(a)) showed a characteristic broad signal near 1560 cm^{-1} due to -C-NH- stretching of amide acid groups. The amide -C=O (CONH) stretching resonance (near 1660 cm^{-1}) overlapped with the ketone stretching of the PMDA [46,47]. The characteristic

peaks of the cyclic anhydride vibrations and acetate located at 1855 cm^{-1} (C=O) and 1236 cm^{-1} (CO-O) indicating that the reactional mixture obtained by reacting with PMDA and D230 still contained unreacted anhydride at room temperature [48,49]. After thermal imidization at 130 °C for one hour, the FTIR spectrum revealed the main characteristic absorptions of the polyimide, such as the strong symmetric imide carbonyl stretching at 1720 cm^{-1}, the imide carbon-nitrogen(C-N) stretching at 1383 cm^{-1} [50]. An additional weaker band at 1772 cm^{-1} and 730 cm^{-1} was found in the asymmetric imide carbonyl stretching and bending vibration [51]. Another strong absorption signal near 1120 cm^{-1} was the signature of ether bonds (C-O-C) from the D230 diamine. The intensity of the 1560 cm^{-1} amide acid (-C-NH-) stretching broad signal weakened rapidly after thermal imidization at 130 °C, which outlined the rapid process of amide-acid cyclization. The FTIR spectra of PEAS exhibited no significant differences between the two polymerization processes, as shown in **Fig. 4** (b). The corresponding prominent infrared absorption peaks of polyimide during synthesis are displayed in **Table S1**. It can be seen from **Fig. 4** (a) that with the increase of thermal imidization temperature, the stretching vibration absorption peak of C=O bond on the imide ring began to appear at 1720 cm^{-1} after 130 °C, indicating the start of imidization reaction. With the increase in temperature, the intensity of this peak gradually increased until it became stable at 230 °C. The reaction degree of the PAA precursor at different thermal imidization temperatures can be calculated according to the characteristic absorption peak area data corresponding to the functional group in the infrared spectrum.

Based on the stability of the benzene ring structure in the reaction process and the significance of the peak in the infrared spectrum, we took the absorption peak of the benzene ring (1500 cm^{-1}) as the benchmark. The degree of imidization reaction was estimated via the relative size of the area of the imide characteristic absorption peak and the absorption peak of the benzene ring. According to the Beer-Lambert rule, the degree of imidization reaction can be calculated by the following formula [52]:

$$RD\% = \frac{S_1(t)/S_0(t)}{S_1(280)/S_0(280)} \times 100\% \quad (3)$$

Where, *RD* is the reaction degree; $S_1(t)$ is the area of the imide symmetric stretching characteristic absorption peak (C=O) at 1720 cm^{-1} at t °C; $S_0(t)$ represents the area of the benzene ring absorption peak at 1500 cm^{-1}. $S_1(280)$ and $S_0(280)$ are the areas of the characteristic absorption peak of imidization and benzene ring absorption peak at 280 °C, respectively.

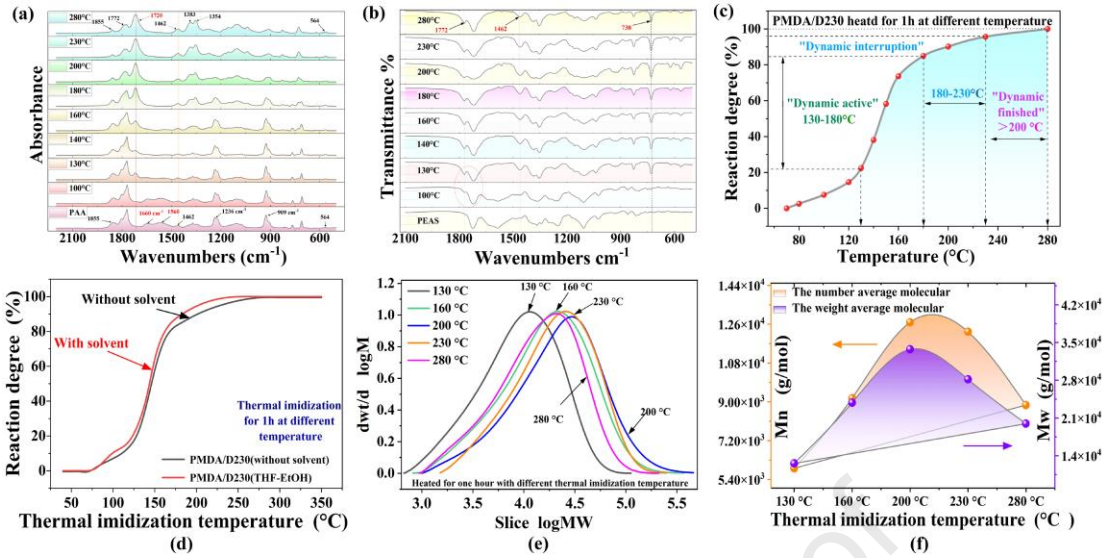

Fig.4. (a) The FTIR spectra of the PAA (PMDA/D230) and (b) the spectra of the PEAS. (c) The reaction degree of imidization (PAA) and (d) comparison with the imidization reaction degree of the PEAS. (e-f) The molecular weight distribution and growth trend of molecular weight.

As shown in **Fig. 4** (c), the imidization reaction degree of PAA was relatively low when the thermal imidization temperature was lower than 130 °C. The degree of imide reaction increased sharply when the temperature exceeded 130 °C. The degree of amide reaction became slow when the temperature exceeded 180 °C (RD > 85 %). It was challenging to continue to improve the degree of imidization reaction even if it stayed at a high temperature for a long time. The reaction degree of polyimide reached 100 % when the thermal imidization temperature was 280 °C. Thus, the thermal imidization reaction of the PAA precursor was completed at 280 °C. According to relevant literature, the reaction temperature range (130-180°C) is called the "Dynamic Active" period, the temperature range of 180-230 °C is called the "Dynamic interruption" period, and the temperature range of 230-280 °C is called "Dynamic termination" period [53-55]. The reaction degrees of synthetic PMDA/D230 PIs synthesized with or without solvent were compared in **Fig. 4**(d), which showed similar trend with the increase of reaction temperature. However, the reaction degree of the PMDA/D230 with solvent was slightly higher than that of PMDA/D230 without solvent. To further investigate whether the thermal imidization temperature of the synthesized polyimide sample was related to the chain structure of polyimide, the molecular weight of different PIs synthesized with solvent (PEAS) was measured. **Figs. 4** (e-f) display molecular weight distribution and growth trend of molecular weight with different thermal imidization temperatures, and their corresponding M_n, M_w, and polydispersity index (PDI) values are listed in **Table 1**. The results demonstrated that the molecular weight increased gradually with the rise of thermal imidization temperature, and the slice logM_w value reached the maximum at 200 °C. The M_n and M_w value of the PI increased from 5,918 to 12,686 g/mol and 12,590 to 33,736 g/mol, respectively, with the increase of imidization temperature from 130 °C to 200 °C. It indicated that the thermal imidization

reaction would intensify the branching structure of the synthesized polyimide segments. The molecular weight multiplication caused by the chain branching mechanism was critical to accelerating the degree of imidization reaction. However, the M_n and M_w values gradually decreased and the peak of the molecular weight curve moved to low molecular weight direction when the temperature exceeded 200 °C, which indicated that high temperature would aggravate the degradation of synthetic polyimide segments. The atoms in the polyimide molecule vibrate more severely at high temperatures, which would cause twisting in the spatial position of the entire polyimide molecular chain. The C-N bond in the imide ring of the polyimide molecule breaks first due to its low bond energy. As the temperature continues to rise, energy gradually accumulates in the PI molecule, leading to multiple chemical bond breaks, followed by the main chain fracture of the PI molecule, which causes a decrease in the degree of polymerization [56,57].

Table 1. The M_n, M_w, and M_w/M_n of the synthetic polyimide with different thermal imidization temperature

No.	Serials	M_n (g/mol)	M_w (g/mol)	M_w/M_n
1	TPI-130 (no solvent)	5,204	10,635	2.04
2	TPI-200 (no solvent)	10,972	24,106	2.19
3	TPI-280 (no solvent)	7,139	15,097	2.11
4	TPI-130 (THF-EtOH)	5,918	12,590	2.13
5	TPI-160 (THF-EtOH)	9,170	23,836	2.59
6	TPI-200 (THF-EtOH)	12,686	33,736	2.66
7	TPI-230 (THF-EtOH)	12,248	28,171	2.30
8	TPI-280 (THF-EtOH)	8,850	19,948	2.25

The chemical shifts (δ) of ^{13}C NMR spectrum for the different compounds are provided in **Table S2** [58-61]. The chemical structures of the PEAS and polyimide are shown in **Fig. 5**. The peak at 168.5 ppm was attributed to the anhydride carbonyl in the PEAS moiety, and the signal at 57.5 ppm was assigned to the -C-OH carbon. After the thermal imidization at 130 °C for one hour, the NMR spectrum revealed the main characteristic signals of polyimide, including the strong signal imide carbonyl at 166.2 ppm, and the imide carbon-nitrogen(C-N) signal at 117.2 ppm. The spectrum of PI thermal imidizated at 200 °C for one hour were slightly intensified, which could be assigned to the change of structure or solubility. In addition, the aromatic carbon multiple signals (1 to 6) were also simplified to five different signals, one being twice as intense as the single others (signals 3 and 6, 126.2 ppm). Such simplification was due to the cyclization of the PEAS isomeric functions to the single imide form [47]. An exciting evolution concerned the signal 12 amide/imide signal. The amide acid -CH resonance was located between 46.1 and 46.6 ppm, while the imide -CH signal was shifted toward 46.5-47.5 ppm. Therefore, the imidization reaction of PEAS was confirmed when the thermal imidization temperature was higher than 130 °C, and no residual PEAS signals could be spotted in the ^{13}C NMR spectra of

the polyimides obtained when the reaction temperature reaches 200 °C.

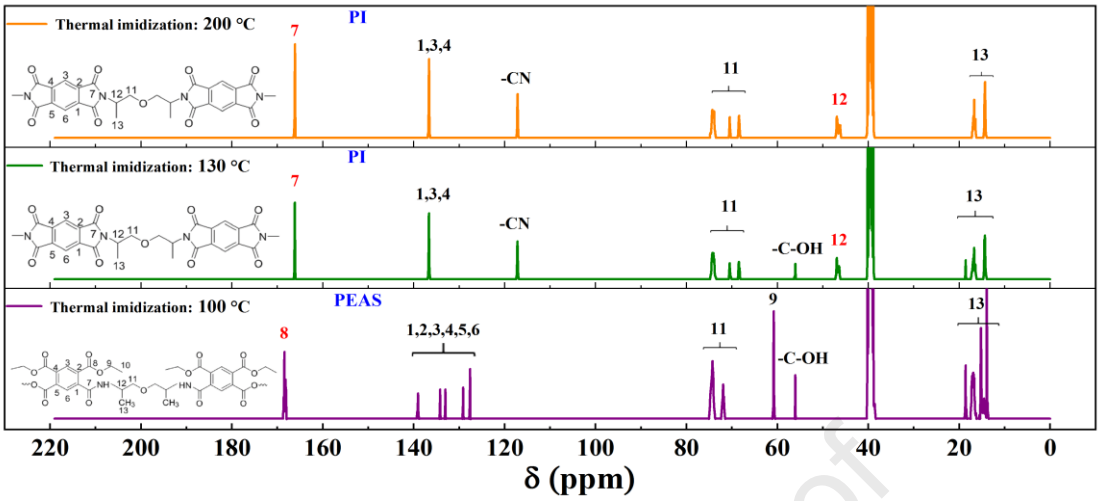

Fig. 5. ^{13}C NMR Spectra (DMSO-D6, 100 °C) of the initial reactive medium (PEAS) and fully cyclized polyimide (thermal imidization temperature at 130 °C and 200 °C for one hour).

3.2. Thermal behavior analysis of the synthetic polyimide

The influence of the imidization temperature on the thermal properties of the PI was investigated. The PAA precursor showed that the glass transition stage was not observed until the second heating cycle (**Fig. 6**(a)). The exothermic peak appeared in the range of 140-200 °C, representing thermal imidization occurred in the first heating cycle. However, there was no exothermic peak during the second heating process, which proved that the thermal imidization reaction had been completed. With the increase in pre thermal imidization time, the T_g shifted to a higher temperature, indicating that thermal imidization reaction time would play a vital role in accelerating the degree of reaction. In addition, the imidization enthalpy gradually decreased with the increase of pre thermal imidization time from 10 to 60 min. Therefore, the longer the reaction time, the better the fluidity of the molecular chain and the sufficient branched reaction. The isothermal DSC measurements on the PAA thermal treated at 140 °C and 150 °C for one hour. As shown in **Fig. 6**(b), it took 0.95 min for the 140 °C heating sample to reach the thermal imidization exothermic peak, while it took only 0.5 min for the 150 °C heating sample, which indicated that the higher the thermal imidization temperature, the shorter time to reach the curing peak and the higher the reaction degree of imide. The DSC exothermic curves of synthetic polyimide with different thermal imidization temperatures are shown in **Fig. 6** (c). The exothermic peak of PAA appeared at 140-180 °C, and the peak shifted to a higher temperature with the increase of thermal imidization temperature, and the area of the exothermic peak was gradually decreased. However, the exothermic curve was straight when the thermal imidization temperature was 280 °C, which means that high temperatures would promote the thermal imidization reaction due to the enhanced reaction activity and the exothermic peak would disappear when the imidization reaction had been completed. The

region of glass transition was shown in **Fig. 6**(f). It was found that the Tg of PAA (83.83 °C) was very close to that of the PMDA (83.86 °C) particle (**Fig. 6**(d)), indicating that some PMDA residues in PAA were not involved in the imidization reaction. The Tg decreased from 83.63 °C to 74.6 °C with the thermal imidization temperature increased from 100 to 140 °C, which manifested that PMDA was gradually consumed. Nevertheless, further increasing the thermal imidization temperature to 200 °C, the Tg was increased to 82.49 °C. This ariation could be attributed to the branching structure generated via the thermal imidization reaction. A branched design could restrict the movement of PI molecular chains, leading to the increase of Tg. Another reason was the increased intermolecular force caused by the spontaneous formation of complexes with hydrogen bonds (H-complexes) between the amino group of the D230 and the carboxylic and ester groups of PMDA [62]. Unfortunately, the Tg value gradually decreased when the thermal imidization temperature exceeded 200 °C. This was because the high temperature would intensify the degradation of synthetic polyimide molecular chain segments.

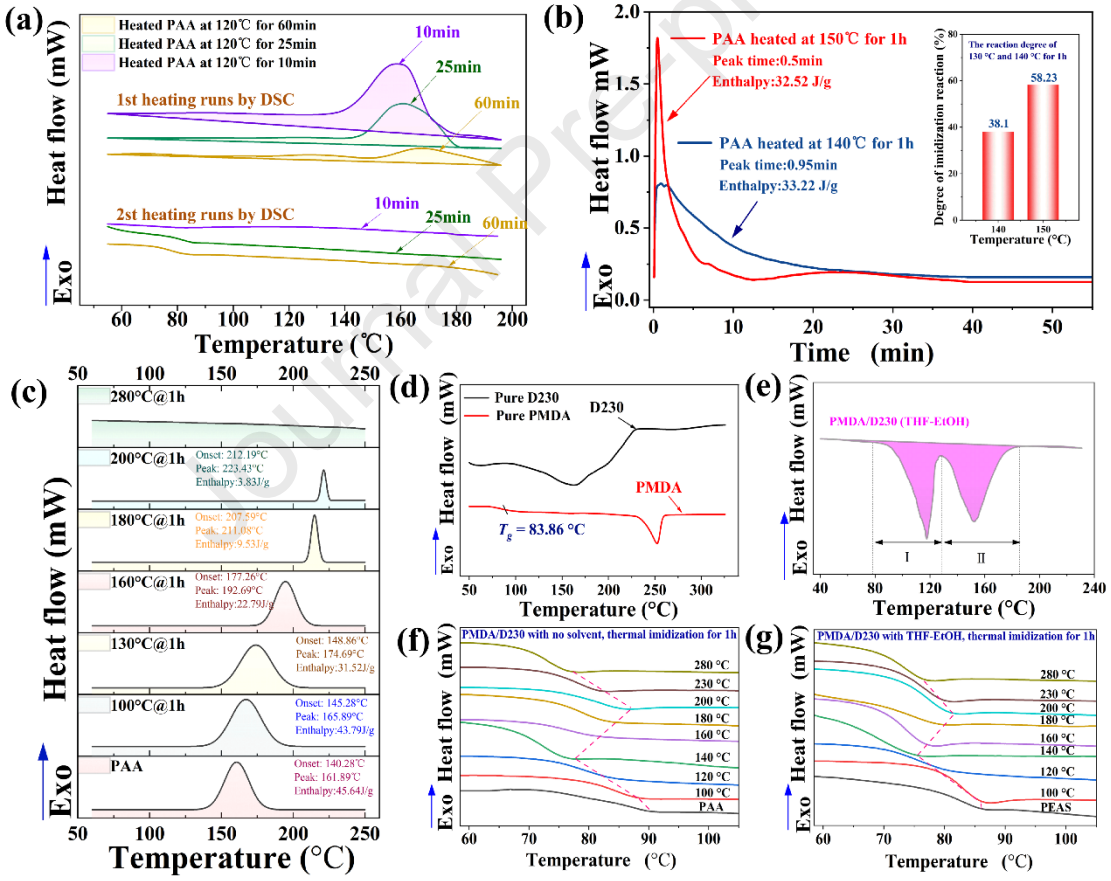

Fig. 6. (a) PAA first and second heating processes with different holding times. (b) Isothermal curves at 140 °C and 150 °C thermal imidization temperature for one hour. (c) The exothermic curves of synthetic polyimide with different thermal imidization temperatures. (d) DSC of PMDA and D230. (e) The DSC curves of the PEAS precursor solution. (f) the Tg curve of PAA. (g) The Tg curve of PEAS.

Fig. 6(e) presents the DSC curves of the PEAS precursor (THF-EtOH) at a heating rate of 4 °C/min from 25 °C to 300 °C. The first exothermic peak (80-130 °C) was mainly the PEAS

precursor's residual THF and EtOH solution. The gases volatilized from the second exothermic peak (130-180 °C) were mainly THF and EtOH molecules bounded by hydrogen bonds, and the water and ethanol molecules separated from the thermal imidization reaction. Analogously, the Tg curves of PEAS with different thermal imidization temperatures are displayed in **Fig. 6**(g). It was found that the glass transition behavior of PEAS and PAA (**Fig. 6**(f)) are very similar. In addition, the Tg of PEAS reduced slightly at 100-140 °C thermal imidization temperature due to the volatilization of THF and EtOH gas, which acted as a plasticizer and weakened the entanglement, leading to the decrease of Tg.

The thermal degradation properties were investigated via the thermogravimetric analysis (TGA) under a nitrogen atmosphere. It can be seen from **Fig. 7**(a) that the degradation temperature of PAA thermal imidization products (160 °C and 200 °C) was lower than that of PEAS. Meanwhile, the maximum decomposition temperatures of PEAS were significantly higher than PAA synthesized at 160 °C and 200 °C thermal imidization temperatures (**Figs.7**(b-c)) according to derivative thermogravimetric (DTG) analysis, indicating that the heat resistance of PEAS was superior to PAA. **Figs. 7**(e-f) show that the PEAS precursor presented two degradation steps. The first step (80-180°C) was mainly attributed to the residual THF and EtOH solvent. The initial decomposition temperature of synthetic polyimide developed positively with the increased thermal imidization temperature. The internal branching structure entanglement network formed at high temperatures would restrict the movement of the polyimide chain segment to a certain degree, hindering heat transfer, lowering the thermal degradation rate, preventing the escape of volatile gas, and improving heat resistance [63]. Nevertheless, the initial thermal degradation temperature gradually moved to low-temperature when the thermal imidization temperature exceeded 200 °C due to the breaking of the molecular chain, which is consistent with the results of DSC and GPC. Analogously, the DTG curve in **Fig. 7**(d) depicts the same trend. It has been demonstrated that the thermal imidization temperature of 200 °C would lead to superior thermal stability of the co-polyimide.

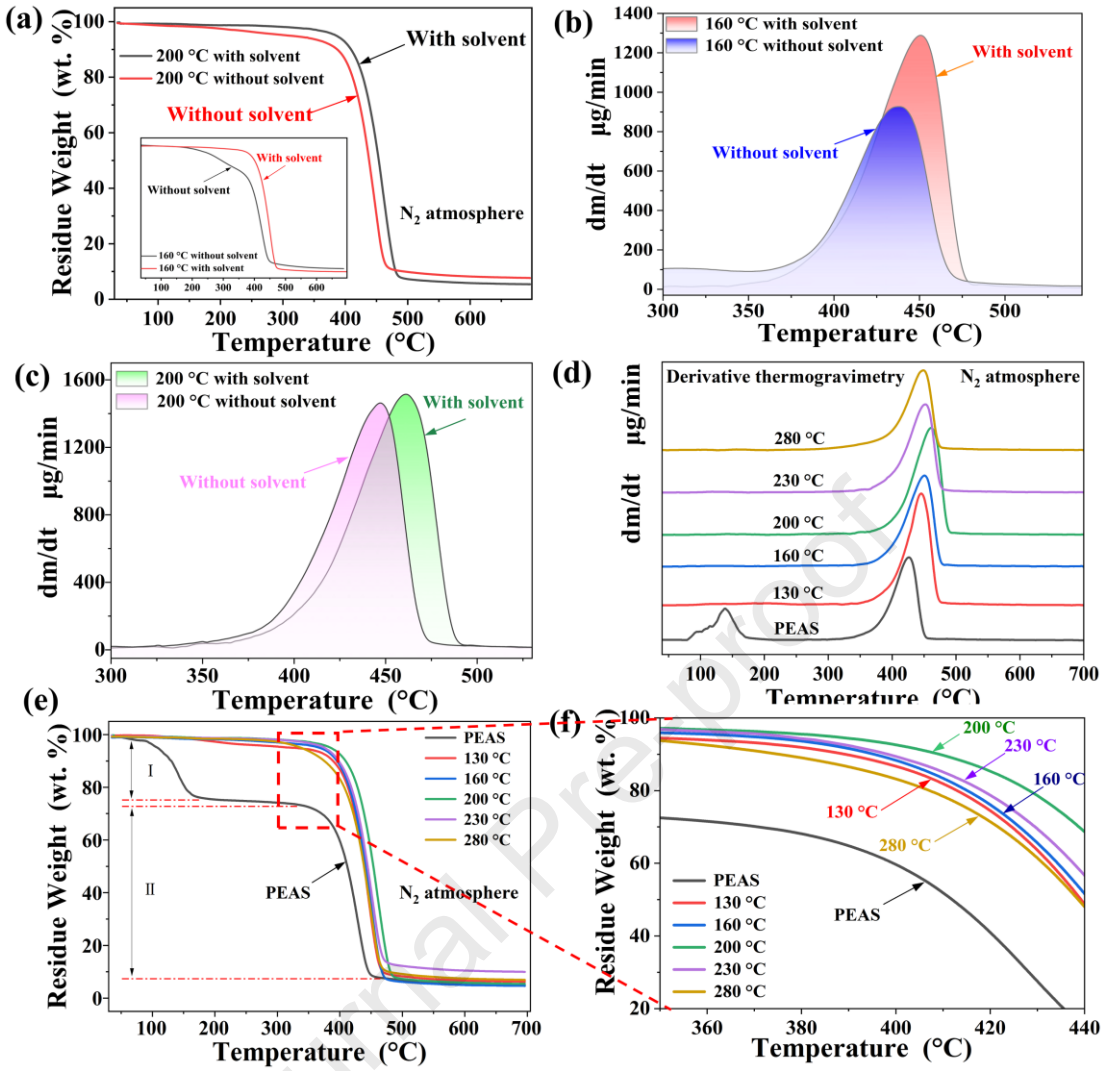

Fig. 7. (a-c) The thermal degradation temperature and DTG curves of PAA and PEAS at the thermal imidization temperature of 160 and 200 °C. (d-e) DTG curves and TGA of PEAS with different thermal imidization temperature. **(f)** magnification of one section of Fig. 7 (e).

3.3. Rheological behavior analysis of the synthetic polyimide

The rheological properties were often positively correlated with the melt strength of the polymer, which was a crucial factor affecting polymer foaming [63,64]. The dynamic frequency sweep tests were carried out to explore the effect of the thermal imidization temperature on melt viscoelastic responses of the synthetic polyimide. **Fig. 8**(a) shows the change of storage modulus (G') with frequency at different thermal imidization temperatures. It could be seen that the G' gradually accumulated and the dependences of G' on frequency became more robust with the increase of thermal imidization temperature at low frequency, reaching the peak when the temperature was 200 °C, then G' decreased with further increase of temperature. A branched network structure might explain the absence of terminal behavior. It has been demonstrated that the branched structure could effectively restrain the large-scale relaxations of the polymer matrix and form a solid-like state that could store the deformation energy [65,66]. Longer

characteristic relaxation time could lead to higher local stress or strain energy, which was beneficial for cell nucleation during the foaming process [67,68]. It was found that the thermal imidization temperature reached a rheological percolation value of 200 °C, which may indicate the degradation of the PI chain segment and the reduction of the branched network [66]. In **Fig. 8**(b), the loss modulus (G'') increased with the thermal imidization temperature from 130-200 °C. The migration of molecular chains required greater external forces due to the tighter entanglement between polyimide chains, resulting in the energy loss needed to increase viscous flow [69]. The reason for the decrease of G'' was similar to **Fig. 8**(a), when the thermal imidization temperature exceeded 200 °C, and the loss of energy needed for viscous flow declined due to molecular chain breaking.

Fig. 8(c) shows the loss factor (tanδ) as a function of frequency for the synthetic polyimide. The tanδ reflected the viscoelasticity of composite materials to a certain extent. It was generally considered that the loss factor was positively related to the viscosity of the material and negatively associated with the material's elasticity. The tanδ of the synthetic polyimides showed a trend of first rising and then falling with the increase of the thermal imidization temperature, indicating that the rise of G'' at low frequencies region was more significant than that of G', while the increase was smaller in the high-frequency region, which was attributed to the internal entanglements caused by the branching structures of the material. In contrast, the entanglement points were destroyed, and the molecular chains were regularly arranged along the shear direction at high frequencies, thus, showing a superior G'. For example, for the PI with thermal imidization temperature of 200 °C, its tanδ showed the highest value at low frequencies, indicating a higher viscosity response. However, it offered better elasticity at high frequencies even the lowest value it has, which should facilitate foaming. Moreover, the changing trend of loss factor showed that linear molecular structure, branched structure, and molecular chain breaking structure in the synthetic polyimide would interact, which promoted the formation of an internal rheological percolation network.

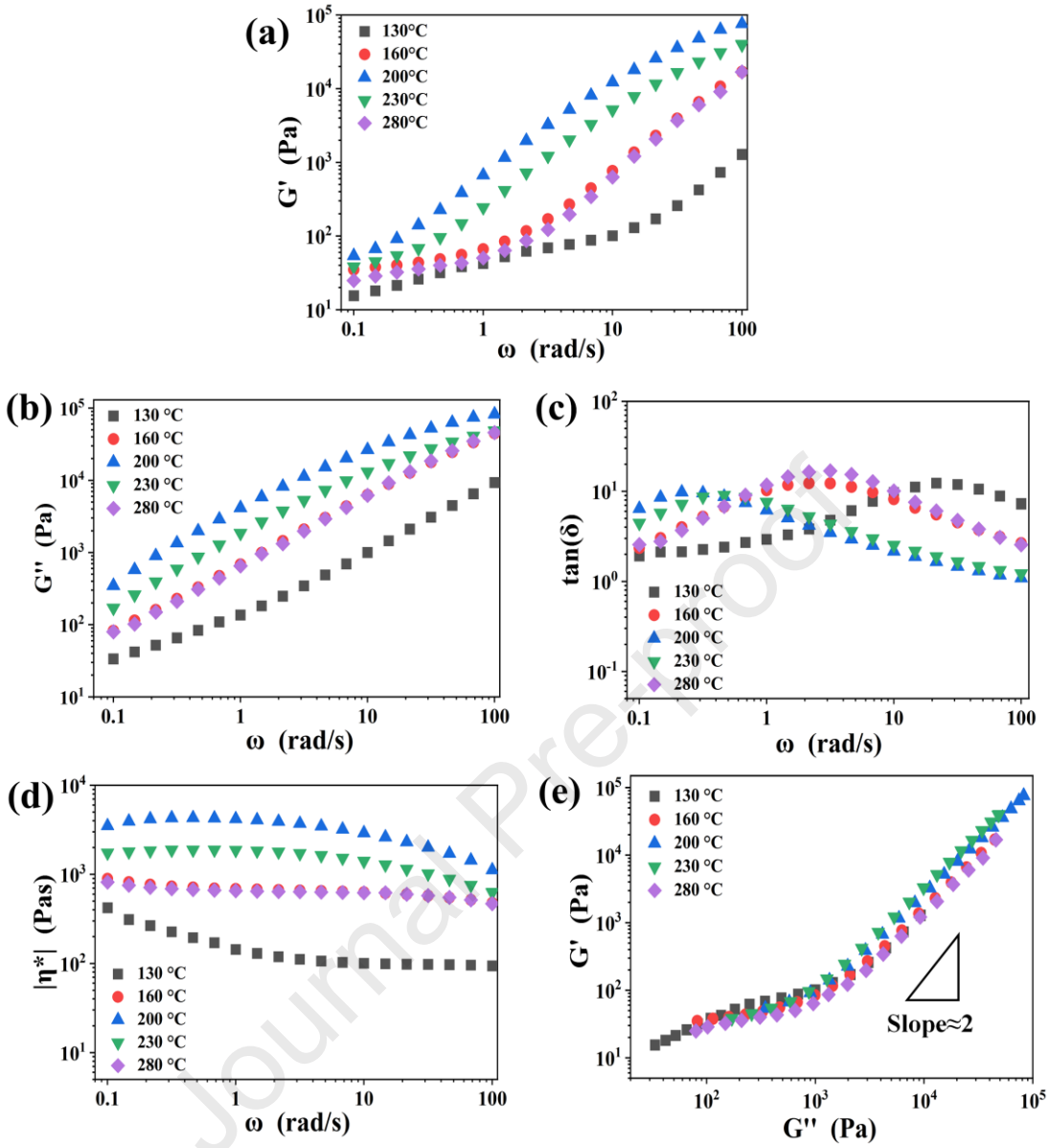

Fig. 8. Rheological behavior of the synthetic polyimide with different thermal imidization temperatures. (a) Frequency dependence of G'. (b) Frequency dependence of G'. (c) frequency dependence of tan δ. (d) Frequency dependence of |η*|. (e) Han plots of G' vs. G''.

Fig. 8(d) displays the complex viscosity (|η*|) as a function of frequency for the synthetic polyimide. It could be reported that |η*| increased gradually with the increase in thermal imidization temperature from 130-200 °C, especially at low frequencies. It demonstrated a strong interaction due to the internal branched structure. The increasing trend of |η*| began to slack and was lower than PI-200 when the thermal imidization temperature overtopped 200 °C (PI-200). This might indicate that it reached a network percolation value when the thermal imidization temperature reached 200 °C. The increasing trend of |η*| was due to the growing molecular entanglements formed by the branched structure. The decreasing |η*| of PI-230 was due to the reduction of a branched network by degradation. The higher |η*| should be beneficial for restraining the bubble from rupturing during cell growth. At high frequencies, |η*| of all

synthetic polyimide decreased, and the decreasing trend became more evident with higher thermal imidization temperature. It was supposed to be the orientation of molecules via the increasing frequency, and the tropism could lead to the disentanglement of the branched structure [70].

Fig. 8(e) shows the G'~ G'' Han plots of the synthetic polyimide with different thermal imidization temperatures. It was found that the G' versus G'' slope of the thermal imidization temperature at 130 °C, 160 °C, 200 °C, 230 °C, and 280 °C decreased at low frequencies, which indicated the need for longer relaxation time for synthetic polyimide chains caused by the internal branched structure. It also signified the presence of branched structure entanglements, which presented inhomogeneity in system [71]. That was beneficial for cell nucleation during the foaming process [72]. The disentanglement of the branched structure at high frequencies caused by the increased shear stress led to the overlap of five curves. Additionally, the slope of the synthetic polyimide at high frequencies was around 2, which indicated that the synthetic polyimide was homogeneously isotropic and behaved in a liquid-like viscoelasticity [65].

3.4. Microcellular structure of the TPIFs

The consequences of the above discussion demonstrated that the thermal imidization temperature affected the properties of the synthetic polyimide system. The melt strength of the polymer is highly dependent on the internal molecular structure and temperature. It was improved when a branching or partial cross-linking network was present, which was conducive to polymer foaming. Nevertheless, the existence of excessive cross-linked structures would inhibit cell growth. The melt strength of the sample was unstable as the temperature exceeded the foaming processing window, and the gas was easy to escape, leading to serious bubble breaking. Therefore, we would probe about the suitable foaming windows of the synthetic polyimide system. According to the foaming results of the preliminary experiment, only about 110 °C could be ideal for foaming, which was the fixed temperature in our experiment. Meanwhile, foaming pressure and time were also crucial factors. To investigate the effect of the thermal imidization temperature, saturation pressure, and time on the foaming behavior of the synthetic polyimide, a solid-state foaming process was carried out on the synthetic polyimide using $scCO_2$ as a physical foaming agent.

The morphologies of the foams were characterized by SEM. **Fig. 9**(a) depicts the foaming process of the sample with thermal imidization temperature at 200 °C for one hour, presenting the cell morphologies with different saturation times (5 min, 10 min, 30 min, and 60 min), the same foaming pressure (10 MPa) and temperature (110 °C). The cross-section of PEAS was very smooth without any impurities and additives, so the foaming process belonged to homogeneous nucleation. At the saturation time of 5 min, the cell shape was approximated circular with a small amount of bubble breaking. The relatively shallow cell depth and thin cell

wall were presented mainly due to the short saturation time which resulted in low CO_2 solubility. The cell size distribution was gradually uniform, the number of damaged cells was reduced, and the bubbles were similar to regular honeycomb hexagons with thick cell walls because of the balanced adsorption and desorption rates of CO_2 at a saturation time of 10min. Meanwhile, the foams with 10 min saturation time possessed a small mean cell diameter (123.78 μm) and the highest cell density (1.12×10^7 cells/cm^3) compared with other foams, as shown in **Fig. 10**(a). However, severe cell collapse and cell wall aggregation were surveyed at a saturation time higher than 30 min. It was believed that the reasons for the cell collapse with increasing saturation time were mainly attributed to the plasticization effect of CO_2. The increasing saturation time cause an increase in the maximum CO_2 uptake for the rigid closed foam [73-75]. The increased CO_2 in the material would affect the matrix's viscosity and foam's expansion, which leaded to the formation of larger cells and weaker cell walls, thus, resulting in the probability of cell merging and cell collapse.

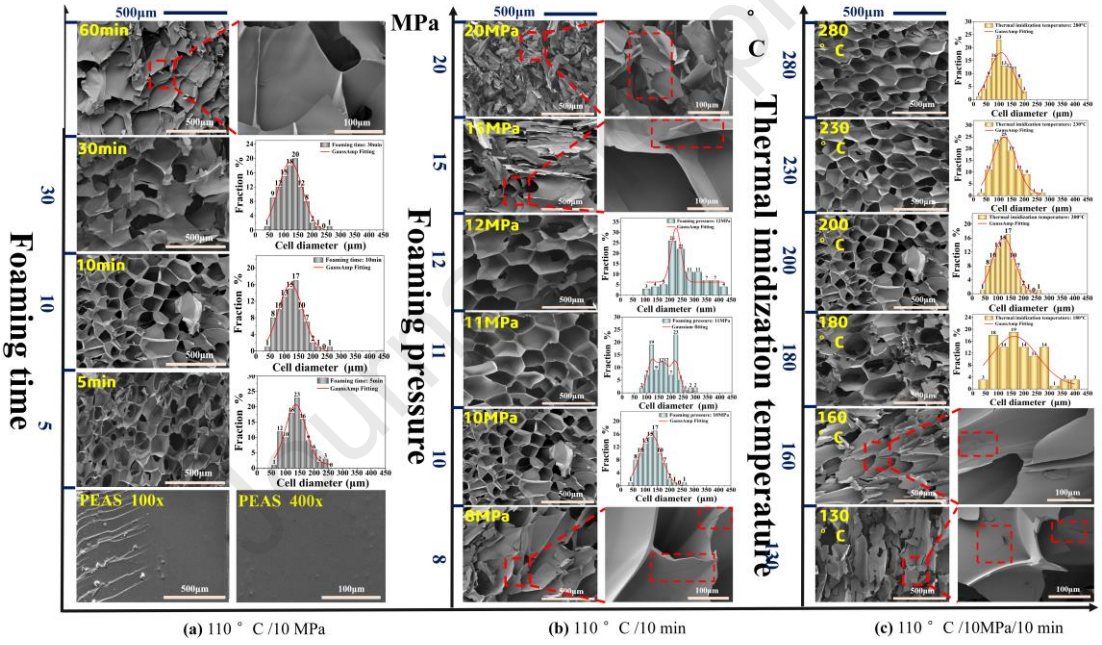

Fig. 9. SEM of the cross-sections of the synthetic polyimide foams and the cell size distribution. (a) Thermal imidization temperature at 200 °C for one hour, with different saturated times. (b) Thermal imidization temperature at 200 °C for one hour, with different saturated pressures. (c) Foaming with different thermal temperatures.

The microstructure of the foams prepared with different saturation pressures is shown in **Fig. 9**(b). When the pressure was 8 MPa, heterogeneous cell structure was obtained owing to the poor nucleation resulting from low CO_2 solubility. As the increase of foaming pressure, the cell size was aggrandized tardily, and the cell density was decreased accordingly (**Fig. 10** (b)). The uniform hexagonal cell structure was presented in the saturation pressure range of 10-12 MPa, indicating a favorable saturation pressure window. Unfortunately, the cell wall was seriously damaged when the pressure exceeded 15 MPa. The poor cell morphology was mainly ascribed to reduced melt strength under high foaming pressure.

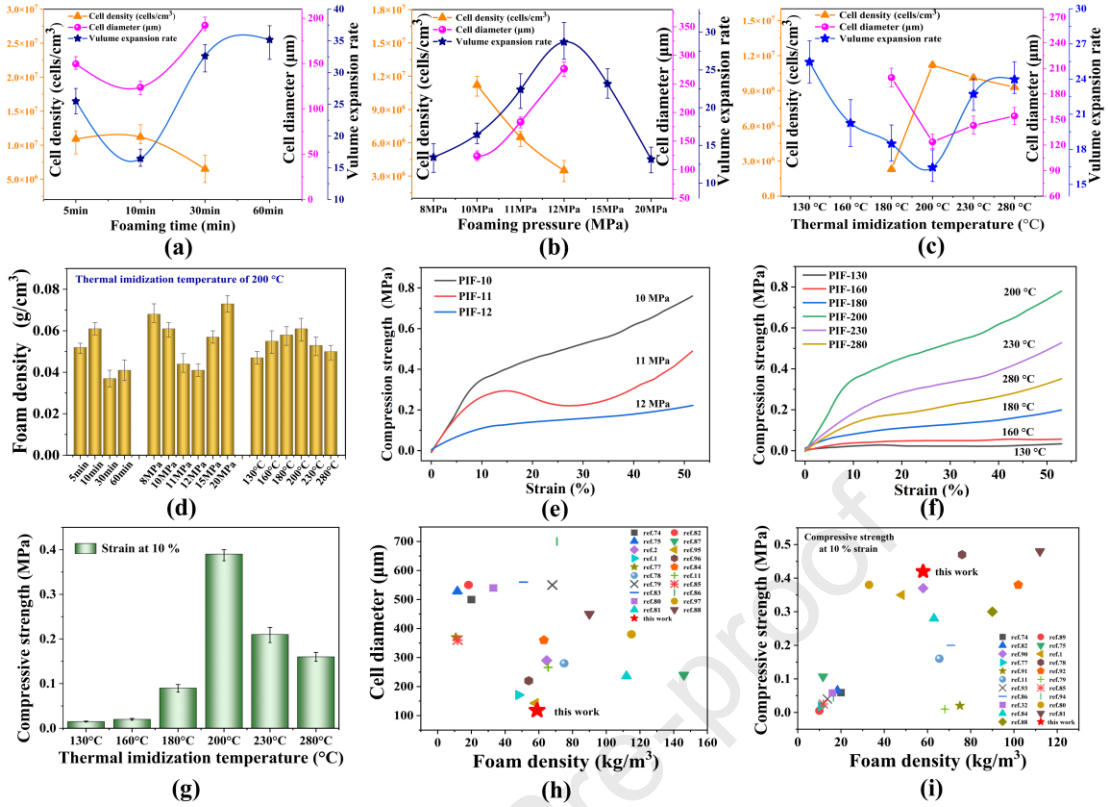

Fig. 10. The data summarization of cell diameter, cell density, and expansion ratio. (a) Different saturated times;(b) different saturated pressures. (c) Different thermal temperatures; (d) foam density. The compressive stress-strain curves of synthetic polyimide with different saturation pressures (e) and different thermal imidization temperatures (f); (g) compressive strength at 10 % strain. (h) Cell size and (i) compressive strength of TPIF compared with those of other foams reported in the literatures.

Severe cell wall aggregation and rupture are observed in the low-temperature region in **Fig. 9**(c). The cell size distribution gradually became uniform, cell wall collapse was significantly reduced, and the number of ruptured cells decreased with the rise of thermal imidization temperature. It is essential to note that the branched structure network has been formed in the synthetic polyimide at a thermal imidization temperature of 200 °C, which could effectively prevent cell fracture and collapse. The melt strength could be improved by slowing down the unwinding process of polymer molecular chain segments [63]. The cell size of PI-200 was remarkably reduced to 123.78 μm compared with the PI-180 foam. A smoother and more uniform low-density microporous polyimide foam could be formed. Although the expansion rate was only 16 times, the cell density was approximately five times higher than PI-180. In addition, the branched structure was helpful to the nucleation of the cell thanks to the increased entanglement network density. With the further increase of thermal imidization temperature, the branched system in the molecule became loose because of the degradation, which gradually increased the cell size and volume expansion rate. It could be inferred that the entanglement point of the branched structure could act as nucleating agents for homogeneous nucleation and improve the foaming properties of the synthetic polyimide. **Fig. 10**(c) presents the cell diameter,

density, and volume expansion ratio of the synthetic polyimide foam with different thermal imidization temperatures at the same saturation temperature, pressure, and time. The foam density obtained under three other foaming conditions is shown in **Fig. 10**(d), and the changing trend was negatively related to the volume expansion rate.

3.5. Mechanical properties of the TPIFs

The compressive stress-strain curve of rigid foam generally consisted of three regions: linear elastic region or Hooke region, platform or collapse region, and densification region [76]. The corresponding compressive stress-strain and strength graphs of TPIFs are shown in **Figs. 10**(e-f). Compared with PIF-12, the compressive strength of PIF-10 was improved by nearly 400 %, as shown in **Fig. 10**(e). The cell size dropped rapidly with the decrease of saturation pressure, which resulted in more cellular skeletons that are sufficient to support higher compressive strength. PIF-10 with optimal cell structure and density presented a high compressive strength of 0.4 MPa at 10 % strain. The compression-strain curve of PIF-11 foam showed a process of first increasing and then decreasing and then climbing up, finally breaking 0.49 MPa under 50 % strain. In the first stage, the linear elastic behavior of closed-cell foams was caused by cell wall bending and stretching by internal gas pressure. In the second stage, the cell collapsed by twisting the cell wall, resulting in decreased strength. The gas in the closed-cell foams was gradually compressed to promote the compaction of foam which caused the rapid increase in compression strength in the third stage. **Fig. 10**(f) indicated that the compressive stress-strain curve of polyimide foam positively correlated with the cell structure. The compressive strength of foam gradually increased with the increase when the thermal imidization temperature was lower than 200 °C. The compressive strength of PIF-200 reached the peak of 0.4 MPa under 10 % strain due to the thicker cell skeleton, as shown in **Fig. 10**(g). The cell structure changed from a hexagonal honeycomb to irregular deformation with the further increase of the imidization temperature, leading to a downward trend in compressive strength. These results demonstrated that preparing PIFs via two-step foaming technology with $scCO_2$ as a foaming agent was a practical approach. Moreover, the mechanical properties could be improved by adequately increasing the thermal imidization temperature and regulating the cellular structure.

Figs. 10(h-i) compare the TPIFs in this study with the rigid thermosetting PIFs in the literature [1,2,8,11,21,32,77-97]. The TPIF with a thermal imidization temperature of 200 °C had the smallest cell size of 123.78 μm at a foaming temperature of 110 °C and pressure of 10 MPa, lower than most thermosetting PIFs reported in the literature. It demonstrated an excellent compressive strength of 0.4 MPa at 10 % strain, which was higher than thermosetting PIFs reported in the literature at the same strain. Thus, TPIFs are promising candidates for meeting the actual demand and commercial use of PIFs. Other reports on preparing TPIFs could not be

found, which indicates that this study addresses a significant gap in the literature.

4. Conclusions

Two TPIs based on PMDA as dianhydride and D230 as diamine have been synthesized through solvent-free blending and solution polymerization methods, respectively. Solvent-free polymerization was found to be challenging to foam due to its low imidization reaction degree and average molecular weight. The PI synthesized using the solution approach had higher molecular weight with the rise of thermal imidization temperature from 130 °C to 200 °C. The optimum thermal imidization temperature defined by DSC and TG analysis was 200 °C. It agrees with the rheological property analysis in which a network percolation value was obtained when the thermal imidization temperature reached 200 °C. TPIFs with microcellular structure and high compressive strength were produced via $scCO_2$ foaming. The cell morphology and mechanical properties of the TPIFs could be turned by varying the saturation time, foaming pressure, and imidization temperature. At a thermal imidization temperature of 200 °C, the TPIFs exhibited a branched structure with a small mean cell diameter (123.78 μm) and a high compressive strength (0.4 MPa) under 10 % strain at a foaming temperature of 110 °C and a pressure of 10 MPa, which was 1000 % greater than that of the TPIFs with thermal imidization temperature of 130 °C. Compared with the rigid thermosetting PIFs reported in the literature, the developed TPIFs had a smaller cell structure and higher compressive strength at the same strain. This work provides feasible means to produce thermoplastic PI foams with tunable microcellular structures and prominent mechanical properties.

CRediT authorship contribution statement

Haiming Liu: Conceptualization, Data curation, Formal analysis, Methodology, Investigation, Methodology, Writing – original draft, Writing – review & editing. **Xiangdong Wang**: Conceptualization, Supervision, Validation. **Hao-Yang Mi**: Formal analysis, Investigation, Validation, Funding acquisition, Writing – review. **Maxwell Fordjour Antwi-Afari**: Writing – review & editing, formal analysis. **Chuntai Liu**: Supervision, Validation, Funding acquisition.

Declaration of competing interest

The authors declare that they have no known competing financial interests or personal relationships that could have appeared to influence the work reported in this paper.

Acknowledgements

The authors would like to acknowledge the financial support of the National Natural Science Foundation of China (52173049). Advantageous Discipline Cultivation Project of Henan Province (222301420032).

References

[1] L. Ni, Y. Luo, X. Peng, S. Zhou, H. Zou, M. Liang, Investigation of the Properties and Structure of Semi-Rigid Closed-Cellular Polyimide Foams with Different Diamine Structures, Polymer 229 (2021) 123957. https://doi.org/10.1016/j.polymer.2021.123957.

[2] Y. Luo, L. Ni, X. Zhang, X. Jiang, H. Zou, S. Zhou, M. Liang, P. Liu, Fabrication of Rigid Polyimide Foams with Superior Compressive Properties, Ind. Eng. Chem. Res. 61 (2022) 1089-1099. https://doi.org/10.1021/acs.iecr.1c04059.

[3] W. Zhai, W. Feng, J. Ling, W. Zheng, Fabrication of Lightweight Microcellular Polyimide Foams with Three-Dimensional Shape by Co2 Foaming and Compression Molding, Ind. Eng. Chem. Res., 51 (2012) 12827-12834. https://doi.org/10.1021/ie3017658.

[4] M. K. A, J. A. P. B. C, K. S. A, M. F. B. B. C, A. P. A, Synthesis of Thermal Insulating Polyurethane Foams From Lignin and Rapeseed Based Polyols: A Comparative Study, Ind. Crop. Prod. 12 (2020) 143. https://doi.org/10.1021/d0704022897368.

[5] A. G. S. de Laia, B. R. Barrioni, T. M. Valverde, A. M. D. Goes, M. D. M. Pereira, Therapeutic Cobalt Ion Incorporated in Poly(Vinyl Alcohol)/Bioactive Glass Scaffolds for Tissue Engineering, J. Mater. Sci. 55 (20) (2020) 8710-8727 . https://doi.org/10.1007/s10853-020-04644-0.

[6] R. Liu, J. Wang, J. Liao, X. Zhang, Robust Silica-Polyimide Aerogel Blanket for Water-Proof and Flame-Retardant Self-Floating Artificial Island, FRONTIERS IN MATERIALS 8 (2021) 659655. https://doi.org/10.3389/fmats.2021.659655.

[7] W. Gu, G. Wang, M. Zhou, T. Zhang, G. Ji, Polyimide-Based Foams: Fabrication and Multifunctional Applications, ACS Appl. Mater. Inter. 12 (2020) 48246-48258. https://doi.org/10.1021/acsami.0c15771.

[8] G. Sun, W. Wang, C. Zhang, L. Liu, H. Wei, S. Han, Fabrication of Isocyanate-Based Polyimide Foam by a Postgrafting Method, J. Appl. Polym. Sci. 134 (14) (2017) 44240. https://doi.org/10.1002/app.44240.

[9] J. Li, N. Yu, Y. Ding, T. Xu, G. Zhang, Z. Jing, X. Shi, Fabrication of Rigid Polyimide Foams with Overall Enhancement of Thermal and Mechanical Properties, J. Cell. Plast. 57 (2021) 717-731. https://doi.org/10.1177/0021955X20956925.

[10] Y. Xu, L. Wang, A. Hu, L. Yuan, Z. Wang, S. Yang, Polyimide Foams for High Temperature Applications, Prog. Chem. 30 (2018) 684-691. https://doi.org/10.7536/PC180220.

[11] H. Liu, H. Tian, Y. Yao, A. Xiang, H. Qi, Q. Wu, A. V. Rajulu, Polyimide Foams with Outstanding Flame Resistance and Mechanical Properties by the Incorporation of Noncovalent Bond Modified Graphene Oxide, New J. Chem. 44 (2020) 12068-12078. https://doi.org/10.1039/d0nj01983f.

[12] Z. Miao, Z. Jia, Z. Yu, S. Chen, S. Zhou, P. Liu, H. Zou, Preparation of Polyimide/Multi-Walled Carbon Nanotubes Composite Aerogels with Anisotropic Properties, J. Appl. Polym. Sci. 137 (2020) 49357. https://doi.org/10.1002/app.49357.

[13] Resewski C , Buchgraber W., Properties of new polyimide foams and polyimide foam filled honeycomb composites, Materialwissenschaft Und Werkstofftechnik 2003 34(4) 365-369. https://doi.org/10.1002/mawe.200390076.

[14] E. S. Weiser, T. F. Johnson, T. L. St Clair, Y. Echigo, H. Kaneshiro, B. W. Grimsley, Polyimide Foams for Aerospace Vehicles, High Perform. Polym. 12 (2000) 1-12. https://doi.org/10.1088/0954-0083/12/1/301.

[15] Barros-Timmons A., Polyurethane Foams: Past, Present, and Future. .Materials (Basel, Switzerland) 11(10) (2018)1841. https://doi.org/10.3390/ma11101841.

[16] Hamidinejad, Mandi, Zhao, Biao, Chu, Raymond, K., M., Moghimian, Nima, Ultralight Microcellular Polymer-Graphene Nanoplatelet Foams with Enhanced Dielectric Performance, ACS Appl. Mater. Inter., 10 (2018) 19987-19998. https://doi.org/10.1021/acsami.8b03777.

[17] Jin-Sek Do,Baoku Zhu,Sang Hyup Han, Synthesis of poly(propylene glycol)-grafted polyimide precursors and preparation of nanoporous polyimides. Polymer International 53 (8) (2004) 1040-1046. https://doi.org/10.1002/pi.1475.

[18] C. Zhang, Q. Lv, Y. Liu, C. Wang, Q. Wang, H. Wei, L. Liu, J. Li, H. Dong, Rational Design and Fabrication of Lightweight Porous Polyimide Composites Containing Polyaniline Modified Graphene Oxide and Multiwalled Carbon Nanotube Hybrid Fillers for Heat-Resistant Electromagnetic Interference Shielding, Polymer, 224 (2021) 123742. https://doi.org/10.1016/j.polymer.2021.123742.

[19] C. Li, C. Zhou, J. Lv, B. Liang, R. Li, Y. Liu, J. Hu, K. Zeng, G. Yang, Bio-Molecule Adenine Building Block Effectively Enhances Electromagnetic Interference Shielding Performance of Polyimide-Derived Carbon Foam, Carbon 149 (2019) 190-202. https://doi.org/10.1016/j.carbon.2019.04.012.

[20] X. Zhang, W. Li, P. Song, B. You, G. Sun, Double-Cross-Linking Strategy for Preparing Flexible,

693 Robust, and Multifunctional Polyimide Aerogel, Chem. Eng. J., 381 (2) (2020) 2-11.
694 https://doi.org/10.1016/j.cej.2019.122784.
695 [21] Y. Luo, L. Ni, L. Yan, H. Zou, S. Zhou, M. Liang, Structure to Properties Relations of Polyimide
696 Foams Derived From Various Dianhydride Components, Ind. Eng. Chem. Res., 60 (26) (2021) 9489-
697 9499. https://doi.org/10.1021/acs.iecr.1c01534.
698 [22] Y. Wang, Z. Zhou, C. Zhou, W. Sun, J. Gao, K. Dai, D. Yan, Z. Li, Lightweight and Robust Carbon
699 Nanotube/Polyimide Foam for Efficient and Heat-Resistant Electromagnetic Interference Shielding
700 and Microwave Absorption, ACS Appl. Mater. Inter., 12 (7) (2020) 8704-8712.
701 https://doi.org/10.1021/acsami.9b21048.
702 [23] Y. Bai, X. Yi, B. Li, S. Chen, Z. Fan, Constructing Porous Polyimide/Carbon Quantum Dots Aerogel
703 with Efficient Photocatalytic Property Under Visible Light, Appl. Surf. Sci., 578 (2022) 1-9.
704 https://doi.org/10.1016/j.apsusc.2021.151993.
705 [24] M. K. Williams, O. Melendez, J. Palou, D. Holland, T. M. Smith, E. S. Weiser, G. L. Nelson,
706 Characterization of Polyimide Foams After Exposure to Extreme Weathering Conditions, J. Adhes.
707 Sci. Technol., 18 (5) (2004) 561-573. https://doi.org/10.1163/156856104839284.
708 [25] C. I. Cano, E. S. Weiser, T. Kyu, R. B. Pipes, Polyimide Foams From Powder: Experimental Analysis
709 of Competitive Diffusion Phenomena, Polymer, 46 (22) (2005) 9296-9303.
710 https://doi.org/10.1016/j.polymer.2005.07.056.
711 [26] P. Joo, Y. Yao, N. Teo, S. C. Jana, Modular Aerogel Brick Fabrication Via 3D-Printed Molds,
712 ADDITIVE MANUFACTURING 46 (2021) 102059. https://doi.org/10.1016/j.addma.2021.102059.
713 [27] Y. Yang, W. Fan, S. Yuan, J. Tian, G. Chao, T. Liu, A 3D-Printed Integrated Mxene-Based Evaporator
714 with a Vertical Array Structure for Salt-Resistant Solar Desalination, J. Mater. Chem. A, 9 (42) (2021)
715 23968-23976. https://doi.org/10.1039/d1ta07225k.
716 [28] Ling-Ying,Pan,Yan-Xia,et al.Visualization study of foaming process for polyimide foams and its
717 reinforced foams, Polymer Composites 31 (1) (2010) 43-50. https://doi.org/10.1002/pc.20764.
718 [29] Weng C J , Jhuo Y S , Huang K Y ,et al.Mechanically and Thermally Enhanced Intrinsically
719 Dopable Polyimide Membrane with Advanced Gas Separation Capabilities, Macromolecules 44 (15)
720 (2011) 6067-6076. https://doi.org/10.1021/ma201130s.
721 [30] Luo Y , Ni L , Zhang C ,et al.Fabrication of Hollow Polyimide Microspheres with Controllable
722 Sizes, Macromolecular Chemistry and Physics 222 (19) (2021) 2100197.
723 https://doi.org/10.1002/macp.202100197.
724 [31]L. Weng, T. Wang, P. Ju, L. Liu, Preparation and Properties of Polyimide/Silver Foams Using a Direct
725 Ion Exchange Method, J. Porous Mat., 24 (2017) 403-409. https://doi.org/10.1007/s10934-016-
726 0273-1.
727 [32]L. Xu, L. Xiao, P. Jia, K. Goossens, P. Liu, H. Li, C. Cheng, Y. Huang, C. W. Bielawski, J. Geng,
728 Lightweight and Ultrastrong Polymer Foams with Unusually Superior Flame Retardancy 9 (31)
729 (2017) 26392-26399. https://doi.org/10.1021/acsami.7b06282.
730 [33] Zhang M B R ,emailprotected, Emailprotected E ,et al.Highly Transparent, Temperature-Resistant,
731 and Flexible Polyimide Aerogels for Solar Energy Collection, ACS Appl. Mater. Interfaces 15 (31)
732 (2023) 37957–37965. https://doi.org/10.1021/acsami.3c07720.
733 [34] Chen B K , Chiu T M , Tsay S Y .Synthesis and characterization of polyimide/silica hybrid
734 nanocomposites, Journal of Applied Polymer Science 94 (1) (2010) 382-393.
735 https://doi.org/10.1002/app.20947.
736 [35] P. Liu, X. Li, P. Min, X. Chang, C. Shu, Y. Ding, Z. Yu, 3D Lamellar-Structured Graphene Aerogels
737 for Thermal Interface Composites with High through-Plane Thermal Conductivity and Fracture
738 Toughness, NANO-MICRO LETTERS, 13 (1) (2021). https://doi.org/10.1007/s40820-020-00548-
739 5.
740 [36] H. C. Liu, A. D. Auguste, J. O. Hardin, A. Sharits, J. D. Berrigan, Additive-Manufactured Stochastic
741 Polyimide Foams for Low Relative Permittivity, Lightweight Electronic Architectures, ACS Appl.
742 Mater. Inter. 13 (23) (2021) 27364-27371. https://doi.org/10.1021/acsami.1c02862.
743 [37] J. Ma, M. Zhan, K. Wang, Ultralightweight Silver Nanowires Hybrid Polyimide Composite Foams
744 for High-Performance Electromagnetic Interference Shielding, ACS Appl. Mater. Inter., 7 (1)
745 (2015) 563-576. https://doi.org/10.1021/am5067095.
746 [38] Kemmere M F , Meyer T .Supercritical Carbon Dioxide (in Polymer Reaction Engineering),
747 Polymer Processing with Supercritical Fluids 23 (2004) 205-238.
748 https://doi.org/10.1002/3527606726.ch10
749 [39] Popescu V , Muresan E I .INDUSTRIAL & ENGINEERING CHEMISTRY RESEARCH, The
750 Society 42(25) (2013) 1559-3584. http://dx.doi.org/10.1111/j.1559-3584.1957.tb03197.x.
751 [40] Matuana, LM, Diaz, and CA, Study of Cell Nucleation in Microcellular Poly(lactic acid) Foamed
752 with Supercritical CO2 through a Continuous-Extrusion Process, Ind. Eng. Chem. Res 49 (2021)

2186-2193. http://dx.doi.org/10.1021/ie9011694.
[41] Reverchon, E. , and R. Adami, Nanomaterials and supercritical fluids, Journal of Supercritical Fluids 37 (2006) 1-22. http://dx.doi.org/10.1016/j.supflu.2005.08.003.
[42] E. Kiran, Supercritical fluids and polymers - The year in review-2014, The Journal of Supercritical Fluids 2 (2016) 1-18. http://dx.doi.org/10.1016/j.supflu.2015.11.011.
[43] O.S. Fleming, and S.G. Kazarian, Polymer processing with supercritical fluids, Supercritical Carbon Dioxide: in Polymer Reaction Engineering, Wiley-VCH Verlag GmbH & Co. KGaA 46 (2004) 205-238. http://dx.doi.org/10.1002/3527606726.ch10
[44] D.L. Tomasko, H.B. Li, D.H. Liu, X.M. Han, M.J. Wingert, L.J. Lee, and K.W. Koelling, A Review of CO_2 Applications in the Processing of Polymers, Ind. Eng. Chem. Res 42 (2003) 6431-6456. http://dx.doi.org/10.1021/ie030199z.
[45] D.L. Tomasko, H.B. Li, D.H. Liu, X.M. Han, M.J. Wingert, L.J. Lee, and K.W. Koelling, A Review of CO_2 Applications in the Processing of Polymers, Ind. Eng. Chem. Res 42 (2003) 6431-6456. http://dx.doi.org/10.1021/ie030199z.
[46] Cho D , Drzal L T .Characterization, properties, and processing of LaRCTM PETI-5 as a high-temperature sizing material. I. FTIR studies on imidization and phenylethynyl end-group reaction behavior.Journal of Applied Polymer Science 75 (2) (2015) 1278-1287. http://dx.doi.org/10.1002/(SICI)1097-4628(20000411)76:2<190::AID-APP8>3.0.CO;2-8.
[47] L. Verny, N. Ylla, F. D. Cruz-Boisson, E. Espuche, V. Bounor-Legaré, Solvent-Free Reactive Extrusion as an Innovative and Efficient Process for the Synthesis of Polyimides, Ind. Eng. Chem. Res. 59 (37) (2020) 16191-16204. http://dx.doi.org/10.1021/acs.iecr.0c02881
[48] Anthamatten M , Letts S A , Day K ,et al.Solid-state amidization and imidization reactions in vapor-deposited poly(amic acid). Journal of Polymer Science Part A: Polymer Chemistry 42 (23) (2004) 5999-6010. http://dx.doi.org/10.1002/pola.20446.
[49] Pryde C A .FTIR studies of polyimides. II. Factors affecting quantitative measurement[J].Journal of Polymer Science Part A: Polymer Chemistry 31 (4) (1993) 1045-1052. http://dx.doi.org/10.1002/pola.1993.080310427.
[50] E. Pyun, R. J. Mathisen, C. Sung, Kinetics and Mechanisms of Thermal Imidization of a Polyamic Acid Studied by Ultraviolet-Visible Spectroscopy, Macromolecules 22 (3) (1989) 1174-1183. http://dx.doi.org/10.1021/ma00193a031.
[51] E. Schab-Balcerzak, H. Janeczek, P. Kucharski, Influence of Azobenzene Units On Imidization Kinetic of Novel Poly(Ester Amic Acid)S and Polymers Properties Before and After Cyclodehydration, J. Appl. Polym. Sci. 118 (5) (2010) 2624-2633. http://dx.doi.org/10.1002/app.32598
[52] G. Guerra, P. Musto, F. E. Karasz, W. J. Macknight, Fourier Transform Infrared Spectroscopy of the Polymorphic Forms of Syndiotactic Polystyrene, Die Makromolekulare Chemie, 191 (9) (1990) 2111-2119. http://dx.doi.org/10.1002/macp.1990.021910914.
[53] Kaas RL. Journal of Polymer Science Polymer Chemistry Edition 1981;19(9):2255-2267. https://www.researchgate.net/publication/287474407_Journal_of_Polymer_Science_Polymer_Chemistry_Edition.
[54] Lillford PJ and Satchell DPN. Journal of the Chemical Society B Physical Organic (1971) 360-374. https://doi.org/10.1039/J297100FP001.
[55] Russell J D , Kardos J L .Modeling the imidization kinetics of AFR700B polyimide[J].Polymer Composites 18(1) (1997) 64-78. https://doi.org/10.1002/pc.10262.
[56] Hatori H , Shiraishi M , Yoshihara M ,et al.The mechanism of polyimide pyrolysis in the early stage, Carbon 34 (2) (1996) 201-208. https://doi.org/10.1016/0008-6223(96)00189-3.
[57] Pramoda K P , Chung T S , Liu S L .Characterization and thermal degradation of polyimide and polyamide liquid crystalline polymers. Polymer Degradation & Stability, 67 (2) (2000) 365-374. https://doi.org/10.1016/S0141-3910(99)00138-X.
[58] Cho D , Drzal L T .Characterization, properties, and processing of LaRCTM PETI-5 as a high-temperature sizing material. I. FTIR studies on imidization and phenylethynyl end-group reaction behavior[J].Journal of Applied Polymer Science, 75 (2) (2015) 1278-1287. https://doi.org/10.1002/(SICI)1097-4628(20000411)76:2<190::AID-APP8>3.0.CO;2-8.
[59] Seshadri K S , Antonoplos P A , Heilman W J .13C-NMR spectroscopy of polyamic acids and polyimides. Journal of Polymer Science Part A Polymer Chemistry 18 (8) (1980) 2649-2662. https://doi.org/10.1002/pol.1980.170180823.
[60] Tina L Grubb, Ulery V L , Smith T J ,et al.Highly soluble polyimides from sterically hindered diamines, Polymer 40 (15) (1999) 4279-4288. https://doi.org/10.1016/S0032-3861(98)00663-6.
[61] J. Sun, Y. Wang, S. Dou, C. Ruan, C. Hu, Peg Derived Hydrogel: A Novel Synthesis Route Under Mild Condition, Mater. Lett. 67 (1) (2012) 215-218. https://doi.org/10.1016/j.matlet.2011.09.075

[62] V. E. Yudin, J. U. Otaigbe, V. N. Artemieva, Processing and Properties of New High-Temperature, Lightweight Composites Based On Foam Polyimide Binder, Polym. Composite., 20 (1999) 337-345. https://doi.org/10.1002/pc.10360.
[63] Y. J. Tang, Z. L. Li, S. H. Chen, X. D. Wang, The Synergistic Effect of Polytetrafluoroethylene in-Situ Fibrillation and Dibenzoyl Sebacate Hydrazide On the Crystallization and Foaming Behavior of Poly (Lactic Acid), Int. J. Biol. Macromol., 221 (2022) 523-535. https://doi.org/10.1016/j.ijbiomac.2022.09.032.
[64] Gao Y N , Wang Y , Yue T N .Superstructure silver micro-tube composites for ultrahigh electromagnetic wave shielding, Chemical engineering journal 430P3 (2022) 2-11. https://doi.org/10.1016/j.cej.2021.132949.
[65] C. Jiang, S. Han, S. Chen, H. Zhou, X. Wang, The Role of Ptfe in-Situ Fibrillation On Pet Microcellular Foaming, Polymer 212 (2020) 123171. https://doi.org/10.1016/j.polymer.2020.123171.
[66] An, Huang, Xiangfang, Peng, Lih-Sheng, Turng, In-Situ Fibrillated Polytetrafluoroethylene (Ptfe) in Thermoplastic Polyurethane (Tpu) Via Melt Blending: Effect On Rheological Behavior, Mechanical Properties, and Microcellular Foamability, Polymer the International Journal for the Science & Technology of Polymers 134 (2018) 263-274. https://doi.org/10.1016/j.polymer.2017.11.053.
[67] J. Zhao, Q. Zhao, C. Wang, B. Guo, C. B. Park, G. Wang, High Thermal Insulation and Compressive Strength Polypropylene Foams Fabricated by High-Pressure Foam Injection Molding and Mold Opening of Nano-Fibrillar Composites, Materials & design 131 (2017) 1-11. https://doi.org/10.1016/j.matdes.2017.05.093.
[68] B. Jza, A. Qz, W. C. Long, C. Cw, G. A. Bing, C. Cbp, C. Gwb, Development of High Thermal Insulation and Compressive Strength Bpp Foams Using Mold-Opening Foam Injection Molding with in-Situ Fibrillated Ptfe Fibers - Sciencedirect, Eur. Polym. J., 98 (2018) 1-10. https://doi.org/10.1016/j.eurpolymj.2017.11.001.
[69] Y. Tang, Y. Wang, S. Chen, X. Wang, Fabrication of Low-Density Poly(Lactic Acid) Microcellular Foam by Self-Assembly Crystallization Nucleating Agent, Polym. Degrad. Stabil. 198 (2022) 109891. https://doi.org/10.1016/j.polymdegradstab.2022.109891.
[70] G. Wang, G. Zhao, L. Zhang, Y. Mu, C. B. Park, Lightweight and Tough Nanocellular Pp/Ptfe Nanocomposite Foams with Defect-Free Surfaces Obtained Using in Situ Nanofibrillation and Nanocellular Injection Molding, Chem. Eng. J. 350 (2018) 1-11. https://doi.org/10.1016/j.cej.2018.05.161.
[71] P. Wang, P. Gulgunje, S. Ghoshal, N. Verghese, S. Kuma, Rheological Behavior of Polypropylene Nanocomposites with Tailored Polymer/Multiwall Carbon Nanotubes Interface, Polymer Engineering & Science 59 (9) (2019) 1763-1777. https://doi.org/10.1002/pen.25176.
[72] P. P Tschke, T. D. Fornes, D. R. Paul, Rheological Behavior of Multiwalled Carbon Nanotube/Polycarbonate Composites, Polymer 43 (11) (2002) 3247-3255. https://doi.org/10.1016/S0032-3861(02)00151-9.
[73] Ali Rizvi,Alireza Tabatabaei,Pouria Vahedi. Non-crosslinked thermoplastic reticulated polymer foams from crystallization-induced structural heterogeneities. Polymer: The International Journal for the Science and Technology of Polymers 135 (2018) 185-192. https://doi.org/10.1016/j.polymer.2017.12.006.
[74]Yaqiao Wang, Xiang Wang, et al. Evolution of cell morphology from sub-macroscale to nanoscale in modified thermoplastic polyether ester elastomer via supercritical CO_2 foaming. The Journal of Supercritical Fluids 171 (2021) 105186. https://doi.org/10.1016/j.supflu.2021.105186.
[75] Forest, C.Chaumont, P.Cassagnau, P.Swoboda, B.Sonntag, P. Polymer nano-foams for insulating applications prepared from CO2 foaming, Progress in Polymer Science 41 (2015) 122-145. https://doi.org/10.1016/j.progpolymsci.2014.07.001.
[76] Mosanenzadeh S G , Saadatnia Z , Shi F ,et al.Structure to properties relations of BPDA and PMDA backbone hybrid diamine polyimide aerogels, Polymer 176 (2019) 213-226. https://doi.org/10.1016/j.polymer.2019.05.050.
[77] L. Ni, Y. Luo, B. Qiu, L. Yan, H. Zou, S. Zhou, M. Liang, and P. Liu, Combining Microwave-Assisted Foaming and Post Curing Process to Prepare Lightweight Flexible Polyimide Foams for Thermal Insulation Applications, Macromol. Mater. Eng 307 (2022) 1-11. https://doi.org/10.1002/mame.202100941
[78] X. Xu, J. Cao, Y. Zhang, F. Yang, and Y. Deng, The synthesis and properties of isocyanate-based polyimide foam composites containing MWCNTs of various contents and diameters, RSC Adv 12 (2022) 5546-5556. https://doi.org/10.1039/d1ra06721d.
[79] H. Liu, Y. Guo, H. Tian, Y. Yao, Q. Liu, A. Xiang, and H. Zhou, Fabrication of polyimide foams

with superior mechanical and flame resistance properties utilizing the graft copolymerization between red phosphorus and graphene oxide, Mater. Sci. Eng. B-Adv 275 (2022) 115498. https://doi.org/10.1016/j.mseb.2021.115498.

[80] L. Yan, L. Fu, Y. Chen, H. Tian, A. Xiang, and A.V. Rajulu, Improved thermal stability and flame resistance of flexible polyimide foams by vermiculite reinforcement. J. Appl. Polym. Sci 134 (2017) 246-259. https://doi.org/10.1002/app.44828.

[81] J. Wu, L. Xia, S. Zhang, and X. Liu, Scalable preparation of individual, uniform hyper-crosslinked polyimide hollow spheres through solid-state powder foaming: The power of network manipulation, MATERIALS TODAY COMMUNICATIONS 24 (2020) 52-65. https://doi.org/10.1016/j.mtcomm.2020.101030.

[82] H. Tian, Y. Yao, W. Liu, K. Wang, L. Fu, and A. Xiang, Polyethylene glycol: An effective agent for isocyanate-based polyimide foams with enhanced foaming behavior and flexibility, High Perform. Polym. 31 (2019) 810-819. https://doi.org/10.1177/0954008318801906.

[83] J. Li, G. Zhang, J. Li, L. Zhou, Z. Jing, and Z. Ma, Preparation and properties of polyimide/chopped carbon fiber composite foams, Polym. Advan. Technol 28 (2017) 28-34. https://doi.org/10.1002/pat.3851.

[84] W. Zhai, W. Feng, J. Ling, and W. Zheng, Fabrication of Lightweight Microcellular Polyimide Foams with Three-Dimensional Shape by CO_2 Foaming and Compression Molding, Ind. Eng. Chem. Res 51 (2012) 12827-12834. https://doi.org/10.1021/ie3017658.

[85] H. Liu, F. Zhao, H. Li, H. Xie, C. Jiang, and L. Xie, Modified hollow glass microspheres composite isocyanate-based polyimide foam with improving mechanical and thermal insulation properties, High Perform. Polym 34 (2022) 465-473. https://doi.org/10.1177/09540083221074606.

[86] J. Li, G. Zhang, Y. Yao, Z. Jing, L. Zhou, and Z. Ma, Synthesis and properties of polyimide foams containing benzimidazole units. RSC Adv 6 (2016) 60094-60100. https://doi.org/10.1039/c6ra08271h.

[87] J. Li, N. Yu, Z. Jing, X. He, X. Shi, and G. Zhang, Fabrication of rigid polyimide foams via thermal foaming of nadimide-end-capped polyester-amine precursor, Polym. Bull 77 (2020) 5899-5912. https://doi.org/10.1007/s00289-019-03045-x.

[88] H. Tian, Y. Yao, S. Ma, L. Fu, A. Xiang, and A.V. Rajulu, Improved mechanical, thermal and flame resistant properties of flexible isocyanate-based polyimide foams by graphite incorporation, High Perform. Polym 30 (2018) 1130-1138. http://dx.doi.org/10.1177/0954008317740195.

[89] X. Chen, X. Sang, and Q. Zhang, Preparation and characterization of polyurethane-imide/kaolinite nanocomposite foams, RSC Adv 5 (2015) 53211-53219. http://dx.doi.org/10.1039/c5ra06438d.

[90] O. Doutres, N. Atalla, M. Brouillette, and C. Hebert, Using shock waves to improve the sound absorbing efficiency of closed-cell foams, Appl. Acoust 79 (2014) 110-116. http://dx.doi.org/10.1016/j.apacoust.2013.12.022.

[91] Y. Luo, Q. Chen, D. Zhu, and M. Matsuo, Graphite Carbon Foam Films Prepared from Porous Polyimide with In Situ Formed Catalytic Nickel Particles, J. Appl. Polym. Sci 116 (2010) 2110-2118. https://doi.org/10.1002/app.31764.

[92] M. Clausi, M. Zahid, A. Shayganpour, and I.S. Bayer, Polyimide foam composites with nano-boron nitride (BN) and silicon carbide (SiC) for latent heat storage, ADVANCED COMPOSITES AND HYBRID MATERIALS 5 (2022) 798-812. https://doi.org/10.1007/s42114-022-00426-1.

[93] Z. Zheng, H. Liu, D. Wu, and X. Wang, Polyimide/MXene hybrid aerogel-based phase-change composites for solar-driven seawater desalination. Chem. Eng. J 440 (2022) 135862. https://doi.org/10.1016/j.cej.2022.135862.

[94] L. Xu, S. Jiang, B. Li, W. Hou, G. Li, M.A. Memon, Y. Huang, and J. Geng, Graphene Oxide: A Versatile Agent for Polyimide Foams with Improved Foaming Capability and Enhanced Flexibility, Chem. Mater. 27 (2015) 4358-4367. https://doi.org/10.1021/acs.chemmater.5b00981.

[95] H. Zhang, H. Zhou, G. Sun, L. Zhang, L. Sun, R. Chen, J. Wang, and S. Han, Easily route to control density of polyimide foams and impact on mechanical and combustion behaviors, J. Cell. Plast 57 (2021) 451-470. https://doi.org/10.1177/0021955X20943111.

[96] Y. Yao, G. Zhang, J. Li, A. Wang, and X. Shi, Effects of 4,4-diaminodiphenyl ether on the structures and properties of isocyanate-based polyimide foams, J. Appl. Polym. Sci 135 (12) (2018) 11-12. https://doi.org/10.1002/app.46029.

[97] Z. Chen, S. Liu H. Huang, J Zhao. Overall improvement in dielectric and mechanical properties of porous graphene fluoroxide/polyimide nanocomposite films via bubble-stretching approach. Materials and Design 117 (2017) 150–156. http://dx.doi.org/10.1016/j.matdes.2016.12.082.

Highlights

1. The poly(amic acid) (PAA) and polyester ammonium salt (PEAS) precursor solutions were synthesized via physical blending and solution polymerization, respectively.

2. Adding a flexible linkage (ether) in the polyimide composite framework reduced the chain order, provided the torsional capacity of the chain segment, and improved its flexibility.

3. Lightweight microcellular thermoplastic polyimide foams (TPIFs) were fabricated via a novel two-step foaming approach using supercritical carbon dioxide ($scCO_2$) as a blowing agent.

4. The branched molecular structure was favourable for improving cell uniformity and mechanical properties.

Declaration of interest statement

We declare that we have no known competing financial and personal relationships with other people or organizations that can inappropriately influence our work, there is no professional or other personal interest of any nature or kind in any product, service and/or company that could be construed as influencing the position presented in, or the review of, the manuscript entitle.